AGU ADVANCING EARTH AND SPACE SCIENCES

Water Resources Research

RESEARCH ARTICLE
10.1029/2025WR041265

Physics-Informed Neural Networks to Develop Site-Specific Pedotransfer Functions

Pengfei Qi[1], Yunquan Wang[1], Rui Ma[1], Jieliang Zhou[2], Harry Vereecken[3], Budiman Minasny[4], Ziyong Sun[1], Gaofeng Zhu[5], and Kun Zhang[6]

[1]Hubei Key Laboratory of Yangtze River Basin Environmental Aquatic Science, School of Environmental Studies, China University of Geosciences at Wuhan, Wuhan, PR China, [2]Institute of Geological Survey, China University of Geosciences, Wuhan, China, [3]Agrosphere Institute, IBG-3, Forschungszentrum Jülich GmbH, Jülich, Germany, [4]School of Life & Environmental Sciences, Sydney Institute of Agriculture, The University of Sydney, Sydney, NSW, Australia, [5]Key Laboratory of Western China's Environmental Systems (Ministry of Education), Lanzhou University, Lanzhou, China, [6]School of Geospatial Engineering and Science, Sun Yat-Sen University, Zhuhai, China

Key Points:

- Traditional PTFs, typically developed on measurements from small-volume soil samples, exhibit limited performance in field applications
- We introduced Site-Specific PTFs (SPTFs), which integrate deep learning with physical modeling of soil hydrologic processes
- SPTFs matched inverse modeling performance while preserving the efficiency of PTFs, based on 1,188 site observations

Supporting Information:

Supporting Information may be found in the online version of this article.

Correspondence to:

Y. Wang,
wangyq@cug.edu.cn

Citation:

Qi, P., Wang, Y., Ma, R., Zhou, J., Vereecken, H., Minasny, B., et al. (2026). Physics-informed neural networks to develop site-specific pedotransfer functions. *Water Resources Research*, *62*, e2025WR041265. https://doi.org/10.1029/2025WR041265

Received 20 AUG 2025
Accepted 31 DEC 2025

Abstract Pedotransfer functions (PTFs) are widely used to estimate soil hydraulic parameters based on easily accessible soil information, playing an important role in the parameterization of earth surface models. However, conventional PTFs, developed using measurements from small volume soil samples, often exhibit significant deviations from field observations and substantial variability when applied to field-scale hydrological models. Here, we introduce new Site-Specific Pedotransfer Functions (SPTFs) that combine deep learning with physics-based modeling of soil hydrological processes. SPTFs differ from conventional PTFs in two aspects: they utilize time-series data as input and they directly optimize simulated soil water content by the 1-D Richardson–Richards equation with observations, ensuring improved applicability to field conditions. We trained and tested the model using two years of soil moisture observations from 1,181 sites in the International Soil Moisture Network. Evaluation using field data demonstrates that SPTFs achieve a Nash-Sutcliffe Efficiency of 0.65 and root mean squared error of 0.072 $cm^3\ cm^{-3}$ in simulating soil water content at the depth of 0.05 m on the test set ($n = 179$), which is close to the values predicted by the inverse modeling method, while maintaining the computational efficiency of PTFs. This study highlights the promise of SPTFs as a robust parameterization framework for localized field applications.

Plain Language Summary Soil hydraulic parameters describe how water moves and is stored in the soil, and they are essential for many hydrological and land-surface models. Traditionally, these parameters are estimated using pedotransfer functions (PTFs), which rely on simple soil descriptions such as texture. However, conventional PTFs are usually built from small laboratory samples, and they often fail to capture how soils behave under real field conditions. In this study, we developed new Site-Specific Pedotransfer Functions (SPTFs) that use both deep learning and physical modeling to provide more accurate parameter estimates for individual field sites. Unlike traditional PTFs, the SPTFs take advantage of time-series soil moisture data and directly match simulated soil water content from the one-dimensional Richards equation to field observations. We trained the SPTFs using 2 yrs of soil moisture measurements from 1,181 global monitoring sites. When tested on independent field data, the SPTFs reproduced soil water content at 0.05 m depth with good accuracy, achieving a Nash–Sutcliffe Efficiency of 0.65 and an error of 0.072 $cm^3\ cm^{-3}$. These findings show that SPTFs can provide both accurate and efficient estimates of soil hydraulic parameters, offering a promising new tool for improving field-scale hydrological modeling.

1. Introduction

Pedotransfer functions (PTFs), which estimate soil hydraulic parameters (SHPs) from easily measured soil characteristics such as texture, have become essential tools for large-scale modeling applications such as land surface models (e.g., Dai et al., 2019; Zhang et al., 2018). PTFs offer a practical alternative to the time-consuming and complex direct measurements of SHPs. Since their conceptual introduction by Bouma (1989), numerous PTFs have been developed to facilitate the estimation of SHPs (e.g., Borgesen et al., 2008; Borgesen & Schaap, 2005; Lamorski et al., 2008; Rudiyanto et al., 2021; Schaap et al., 2001; Wang et al., 2022; Weber et al., 2020; Zhang & Schaap, 2017).

PTFs are typically constructed based on specific hydraulic models and calibrated using laboratory measurements of SHPs. However, as reviewed by Vereecken et al. (2010), Van Looy et al. (2017), and more recently by Weber et al. (2024), such PTFs suffer from several critical limitations. First, they are predominantly developed from small-sample laboratory measurements obtained from diverse locations (e.g., Rudiyanto et al., 2021; Schaap et al., 2001; Schaap & Leij, 1998; Wang et al., 2022; Zhang & Schaap, 2017), which may poorly capture the heterogeneity encountered in field conditions. Second, the input variables commonly used, such as soil texture, bulk density (Schaap et al., 2001; Wang et al., 2022; Zhang & Schaap, 2017), organic matter content (Rawls & Brakensiek, 1982; Vereecken et al., 1989), and soil chemical properties (Tóth et al., 2015), are insufficient to fully represent the effects of soil structure that strongly controls SHPs (Fatichi et al., 2020; Van Looy et al., 2017; Vereecken et al., 2022; Weber et al., 2024). As a result, PTFs often perform poorly when applied in field-scale simulations of soil water dynamics. Several studies have consistently shown substantial variability of different PTFs in predicting SHPs (Nasta et al., 2021; Van Looy et al., 2017; Vereecken et al., 2010), introducing considerable uncertainty into simulations of soil water fluxes (Chirico et al., 2010; Vereecken et al., 1992; Weihermuller et al., 2021) and related processes such as soil carbon cycling (Paschalis et al., 2022). These issues highlight a persistent gap between the parameter estimation capabilities of PTFs and their effective application in modeling efforts (Baroni et al., 2010; Nasta et al., 2021; Turek et al., 2025).

In contrast, inverse modeling has been widely adopted to estimate SHPs for site-specific conditions using process-based models, consistently demonstrating strong performance in both field and laboratory settings (e.g., Bandai & Ghezzehei, 2022; Guo et al., 2024; Li et al., 2024; Taccari et al., 2024; Tsai et al., 2021). However, inverse modeling lacks the predictive efficiency of PTFs, as it typically requires hundreds to thousands of forward model runs for each site to obtain optimal parameter estimates. This computational demand becomes particularly burdensome when complex, nonlinear models are employed, where numerical convergence may not always be guaranteed (Zhu et al., 2018). Despite recent efforts to accelerate inverse modeling through surrogate modeling techniques such as physics-informed neural networks (PINNs; Bandai & Ghezzehei, 2021, 2022) and neural operator learning (e.g., Guo et al., 2024; Taccari et al., 2024), these approaches still depend on underlying process models, thus are unable to fully decouple parameter estimation from the computational burden of forward simulations.

Recently, Tsai et al. (2021) proposed a novel differentiable parameter learning (dPL) framework, which leverages machine learning, specifically, the Long Short-Term Memory (LSTM) network (Hochreiter & Schmidhuber, 1997), to directly estimate model parameters from raw input data, including both static properties (e.g., soil texture, bulk density) and dynamic observations (e.g., meteorological forcing, soil water content time series). The estimated parameters are subsequently incorporated into a differentiable implementation of the process model, in this case, the Variable Infiltration Capacity model (Liang et al., 1994), as applied by Tsai et al. (2021). If the original model is not differentiable, a neural network-based surrogate can be constructed to ensure compatibility within the dPL framework. This framework is trained by minimizing the discrepancy between model outputs and observed data, and once trained, it can rapidly and accurately estimate parameters for new sites without running the process model, similar to PTFs (Li et al., 2024). At the same time, the estimated parameters remain consistent with the target process model, preserving the key advantage of inverse modeling (Kraft et al., 2022; Li et al., 2024; Tsai et al., 2021). Thus, the dPL approach unifies the efficiency of traditional PTFs with the reliability of inverse modeling.

In this study, we aim to develop a new Site-specific Pedotransfer Functions (SPTFs) for rapid and accurate estimation of field-representative SHPs, using the dPL framework. While Tsai et al. (2021) primarily demonstrated the efficiency of the dPL framework in calibrating model parameters, our focus here is on its predictive capability, specifically, the ability of SPTFs to estimate SHPs at previously untrained sites. The development of SPTFs departs from traditional PTFs in two ways. First, SPTFs are trained on site-specific data that combines static soil information and dynamic environmental variables, ensuring robustness in field applications. Second, rather than fitting parameters to laboratory SHP data sets, SPTFs are optimized against simulated soil water content profiles derived from the one-dimensional soil water flow model described by the Richardson–Richards equation. In addition, we assess the influence of two distinct soil hydraulic models on SPTF performance: the widely used capillarity-based van Genuchten–Mualem (VGM) model (Mualem, 1976; Van Genuchten, 1980), and the Fredlund–Xing–Wang model (FXW-M3; Fredlund & Xing, 1994; Wang et al., 2023, 2025), which explicitly accounts for the effects of soil structure and adsorption forces. Once trained, the SPTFs can instantly

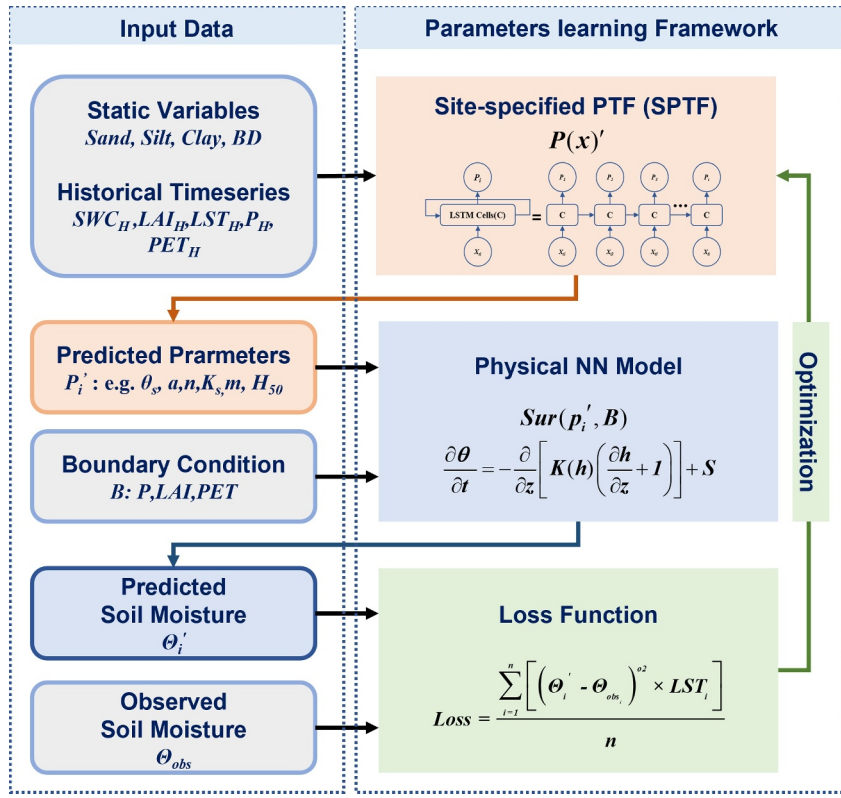

Figure 1. Framework for SPTF development. It involves four aspects: (1) the input information, (2) the SPTF, which is essentially a Long Short-Term Memory model, (3) Neural network-based surrogate model of the 1-D soil water flow model, and (4) the loss function, which is defined as the error between the simulated and observed soil water content across different field sites.

estimate SHPs from site-specific input data, as traditional PTFs do, while also ensuring the estimated SHPs could simulate soil water content dynamics at the field scale, similar as inverse modeling method.

2. Methods and Data

2.1. Framework of SPTF Development

We employed a differentiable parameter learning (dPL) framework, as introduced by Tsai et al. (2021), designed to estimate parameters by accommodating both static and time-series variables. As illustrated in Figure 1, the training process is structured into three main components: (a) the SPTF module P $(X_S, X_H)'$, (b) the Neural Network-based Surrogate model Sur (p_i', B)), and (c) the Loss Function $Loss$.

The SPTF module is a neural network (Figure 1) that estimates SHPs from the input data and can be expressed as:

$$p_i' = P(X_s, X_H)' \tag{1}$$

where P $(X_S, X_H)'$ denotes the untrained SPTF; p_i' is the predicted site-specific parameters, including SHPs and the root water uptake parameter H_{50} (the water potential at which root water uptake rate decreases to 50%, as detailed in Section 2.2). The input variables comprise both static variables (X_S), namely soil texture and bulk density from the surface to 0.05 m depth, and historical time-series variables (X_H), including daily historical soil water content observation at depth of 0.05 m (SWC_H), historical daily leaf area index data (LAI_H), historical daily potential evapotranspiration data (PET_H), historical daily land surface temperature data (LST_H) and daily precipitation (P_H).

Table 1
Constraints Applied for Soil Hydraulic Parameters When Training the SPTF

Parameter	SPTF of FXW-M3	Parameter	SPTF of VGM
θ_s ($cm^3\ cm^{-3}$)	0.32–Max (0.41, max(Θ_{obs}))	θ_r ($cm^3\ cm^{-3}$)	0–0.15
α (cm^{-1})	0.0015–0.2	θ_s ($cm^3\ cm^{-3}$)	0.32–Max (0.41, max(Θ_{obs}))
n	1.05–13.5	α (cm^{-1})	0.0015–0.23
m	0.2–1.6	n	1.05–8
K_s (cm d^{-1})	0.5–8,000	K_s (cm d^{-1})	0.3–8,000
H_{50} (cm)	−50 to −2,000	H_{50} (cm)	−50 to −2,000

Once the predicted parameters p^i are obtained, they are directly fed into the neural network-based surrogate model to simulate soil water content at 0.05 m depth. Here, the neural network-based surrogate model serves as a surrogate for a 1-D soil water flow model, represented by a neural network. It is defined as:

$$\Theta_i' = Sur\left(p_i', B\right) \tag{2}$$

where $Sur\ (p_i', B)$ denotes the neural network-based surrogate model, B is the boundary condition. The predicted soil water content at 0.05 m is denoted by Θ_i', which is then used in the loss function to compute the training error.

The *Loss* function is expressed as:

$$Loss = \frac{\sum_{i=1}^{n}\left[\left(\Theta_i' - \Theta_{obs_i}\right)^{\circ 2} \times bLST_i\right]}{n} \tag{3}$$

where Θ_{obs} is soil water content observation at the depth of 0.05 m for the target period, n is the number of observations. bLST is a binarized index derived from land surface temperature. For LST ≥ 0°C, bLST was set to 1, whereas for LST < 0°C, it was assigned a value of 0 to indicate frozen conditions. The use of bLST is because the soil water model applied in this study does not account for freeze–thaw effects.

It is important to note that the time-series data input to $P\ (X_S, X_H)$ (Equation 1) is from the initial year (i.e., historical data), whereas the input to Sur (p_i', B) (Equation 2) is the target period data of the subsequent year. Although both inputs are of the same type, their time ranges do not overlap, thereby ensuring that the parameters predicted by the SPTF are robust for future use. Table 1 lists the constraints on the output range of SPTF.

The loss function (Equation 3) was minimized using the backpropagation algorithm in conjunction with the Adam optimizer. Given that $P(X_S, X_H)'$ processes time-series data, we adopt a single-layer LSTM model, consistent with Tsai et al. (2021), with a hidden size of 128, an input size of 7, and an output size of 6 as the base architecture. The Adam optimization algorithm is applied with a fixed learning rate of 0.0001, and the training is conducted over 5,000 iterations. The model exhibiting the best performance on the validation set is selected as the final model.

Upon completion of training, the evaluation on the test set is used to assess the generalization performance of the trained SPTFs. A detailed description of the data set can be found in Section 2.5. Since site-specific measurements of SHPs were unavailable, the performance of the SPTFs was evaluated by comparing simulated soil water content that computed using SHPs predicted by the SPTFs with observed values from both the training and test data sets. The SPTF is a neural network whose training process incorporates the physics-based one-dimensional Richardson–Richards Equation, thereby making it essentially a physics-informed neural network.

2.2. Development of the Neural Network-Based Surrogate Model

The dPL framework requires a physics-based model, that is, differentiable to enable backpropagation (Werbos, 1990). To meet this requirement, we first implemented a one-dimensional soil water flow model based on the Richardson–Richards equation (Richards, 1931; Richardson, 1922), and subsequently developed a neural network-based surrogate model trained to replicate the behavior of the Richardson–Richards soil water model.

2.2.1. 1-D Soil Water Flow Model

The physical model is based on the one-dimensional Richardson-Richards equation (Richardson, 1922; Richards, 1931), which incorporates Darcy's law and mass conservation. The governing equation is:

$$\frac{\partial \theta}{\partial t} = \frac{\partial}{\partial z}\left[K(h)\left(\frac{\partial h}{\partial z} + 1\right)\right] + S \tag{4}$$

where t is time (d); z is the spatial coordinate (positive upward) (cm), h is the matric potential (cm), θ is the volumetric water content ($cm^3\ cm^{-3}$), $K(h)$ is the hydraulic conductivity ($cm\ d^{-1}$) and S is the sink term representing root water uptake.

Solving Equation 4 requires specifying a soil hydraulic model, a root water uptake model, initial conditions, and boundary conditions. To simplify the physical model, we set the initial conditions for all sites to a potential of −100 cm.

(1) *Soil Hydraulic Models*

Two soil hydraulic models were used to develop the SPTFs: the capillarity-based VGM model (Mualem, 1976; Van Genuchten, 1980) and the FXW-M3 model (Fredlund & Xing, 1994; Wang et al., 2023, 2025), which accounts for capillary, adsorption, and soil structure effects.

The VGM model is widely used and is expressed as:

$$\begin{cases} S_e(h) = \dfrac{\theta - \theta_r}{\theta_s - \theta_r} = [1 + |\alpha h|^n]^{-m} \\ K_L = K_s S_e^l \left[1 - \left(1 - S_e^{\frac{1}{m}}\right)^m\right]^2 \end{cases} \tag{5}$$

where S_e is the effective saturation degree (unitless), K_L is the liquid water hydraulic conductivity, θ_s and θ_r are the saturated and residual water content ($cm^3\ cm^{-3}$), respectively, α (cm^{-1}), n, and m (=1–1/n) are fitting parameters. l is set to 0.5

The FXW-M3 model is expressed as:

$$\begin{cases} S(h) = \left[1 - \dfrac{\ln(1 + h/h_r)}{\ln(1 + h_0/h_r)}\right]\Gamma(h) \\ \Gamma(h) = (\ln(e + |\alpha h|^n))^{-m} \end{cases} \tag{6}$$

$$K(h) = \begin{cases} K(h_a)\left(\dfrac{\Gamma(h) - \Gamma(h_0)}{\Gamma(h_a) - \Gamma(h_0)}\right)^l \left[\dfrac{1 - \left(1 - \Gamma(h)^{\frac{1}{m}}\right)^{1-1/n}}{1 - \left(1 - \Gamma(h_a)^{\frac{1}{m}}\right)^{1-1/n}}\right]^2 & h < h_a \\ K_s \Gamma(h)^{\frac{\ln(K(h_a)/K_a)}{\ln(\Gamma(h_a))}} & h \geq h_a \end{cases} \tag{7}$$

where S is the saturation degree (unitless); h_a is the critical matric potential distinguishing the impact of soil structure and texture, set to −16 cm (Wang et al., 2023); h_r is a shape parameter, set to -1.5×10^4 cm (Fredlund & Xing, 1994); h_0, corresponding to zero water content, is set to -6.3×10^6 cm (Schneider & Goss, 2012); l has a default value of 3.5; K_a, the saturated matrix hydraulic conductivity, is expressed as:

$$K(h_a) = \min\left\{\theta_s b(h_m)\Gamma(h_m)\left(\frac{\Gamma(h_a) - \Gamma(h_0)}{\Gamma(h_m) - \Gamma(h_0)}\right)^l \left[\frac{1 - \left(1 - \Gamma(h_a)^{\frac{1}{m}}\right)^{1-\frac{1}{n}}}{1 - \left(1 - \Gamma(h_m)^{\frac{1}{m}}\right)^{1-\frac{1}{n}}}\right]^2, K_s\right\} \tag{8}$$

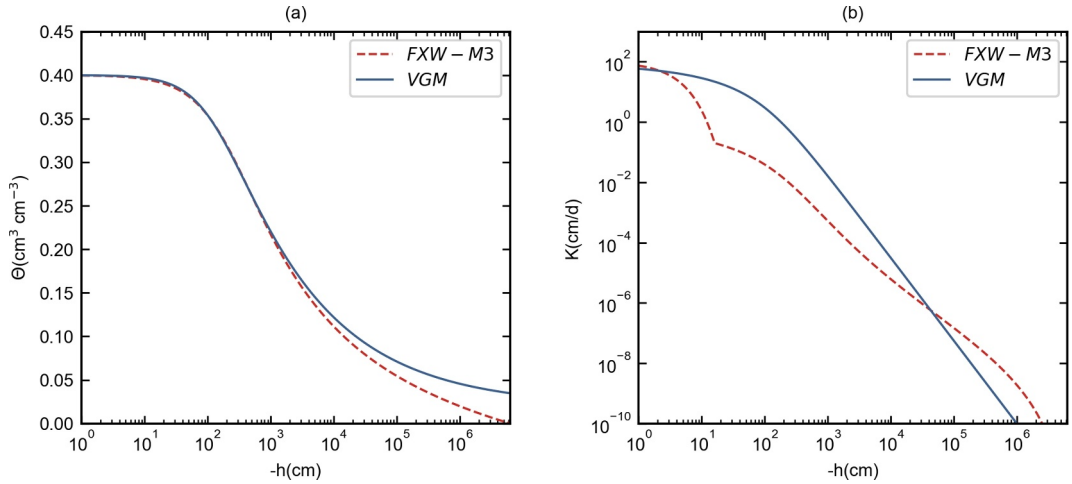

Figure 2. Illustration of the SWRCs (a) and HCCs (b) of both the FXW-M3 and van Genuchten–Mualem (VGM) models. The parameters of FXW-M3 are set to 0.4, 0.006 cm–1, 0.66, 1.1 and 100 cm d–1 for θ_s, α, m, n, and Ks, respectively; and the parameters of VGM are set to 0.4, 0.02 cm–1, 0.006, 1.3,100 cm d–1 for θ_s, θ_r, α, n, Ks, respectively.

where h_m, a typical matric potential where van der Waals forces dominate, is set to -1.0×10^5 cm; $b(h_m)$ is a combined factor representing film thickness and specific surface area, set to 2.693×10^{-6} cm d^{-1} (Wang et al., 2023).

Figure 2 illustrates the differences between the FXW-M3 and VGM models in describing the SWRC and HCC. By considering the additional effect of adsorption forces, the FXW-M3 model predicted a lower θ and higher K in the dry range compared to the VGM model. The FXW-M3 model also shows a distinct bimodal HCC near saturation due to the inclusion of soil structure effects, whereas the VGM model tends to overestimate K and fails to capture bimodal HCC. A detailed comparison and discussion of the FXW-M3 and VGM models can be found in Wang et al. (2023).

(2) *Root Water Uptake Model*

To minimize the number of free-fitted parameters, a simplified S-shaped model (Van Genuchten, 1987) is used to describe root water uptake term S, written as:

$$S(h, h_\varphi) = \lambda(h, h_\varphi)\, S_p \tag{9}$$

where λ is a prescribed dimensionless function of the soil water pressure head; S_p is potential water uptake rate (cm d^{-1}); h_φ is the osmotic head. Here, we do not consider the effect of solute potential and h_φ is set to zero.

λ is expressed as:

$$\lambda(h, h_\phi) = \frac{1}{1 + \left(\frac{h}{H_{50}}\right)^p} \tag{10}$$

where H_{50} represents the matric potential at which the water extraction rate is reduced by 50% under negligible osmotic stress; p is coefficient and set to 3 as default (Van Genuchten, 1987).

A linear root distribution function (Hoffman & Van Genuchten, 1983) is used to describe S_p, written as:

$$S_p = b(x)\, T_p \tag{11}$$

$$b(x) = \begin{cases} \dfrac{1.667}{L_R} & x > L - 0.2L_R \\ \dfrac{2.0833}{L_R}\left(1 - \dfrac{L - x}{L_R}\right) & x \in (L - L_R; L - 0.2L_R) \\ 0 & x < L - L_R \end{cases} \quad (12)$$

where $b(x)$ is the normalized water uptake distribution; T_p is the is the potential transpiration rate (m d^{-1}); L_R is the depth of the root zone (m).

The calculation of T_p depends on the PET and LAI (Ritchie, 1972), written as:

$$T_P = \mathrm{PET}\left(1 - e^{-k * \mathrm{LAI}}\right) \quad (13)$$

where k is a constant governing the radiation extinction by the canopy as a function of sun angle, the distribution of plants, and the arrangement of leaves (set to the default value of 0.39). Notably, since the optimized target is the soil water content at a depth of 0.05 m, which is less influenced by root water uptake, we simplified the current SPTF development by assuming a fixed root depth of 40 cm for all sites. To account for site-specific variations, we treated H_{50} as a free-fitted parameter.

(3) *Boundary Conditions*

The upper boundary condition is set as the system-dependent boundary condition (Neuman et al., 1974):

$$q_{\mathrm{top}}(t) = \min\left[-K\frac{\partial h}{\partial x} - K, E\right] \quad h_A \le h \le h_S \quad (14)$$

where E (cm d^{-1}) is the potential soil evaporation rate and is calculated by:

$$E = \mathrm{PET}\left(e^{-k * \mathrm{LAI}}\right) - P \quad (15)$$

and h_A and h_S are the minimum and maximum matric potential allowed at the soil surface, respectively; h_S is set equal to zero, and h_A is set to the default value of -1.0×10^5 cm.

The lower boundary condition is set as free drainage, representing a unit gradient discharge rate, calculated as:

$$q_{\mathrm{bottom}} = -K(h) \quad (16)$$

where q_{bottom} is the discharge rate at the bottom boundary.

This water flow model was solved using Hydrus-1D (Šimůnek et al., 2008), an open-source finite element solver for water, heat and solute transport in one-dimensional variably saturated media. Notably, for the FXW-M3 model, we modified the source code of Hydrus-1D. Table 2 summarizes the general parameter settings in relation to the soil water flow model.

2.2.2. Construction of the Surrogate Model

Due to the inherent complexity and non-differentiability of the numerical model, a LSTM network was trained as a surrogate model. The neural network-based surrogate model predicts dynamic soil water content at a depth of 0.05 m, utilizing boundary conditions and SHPs as inputs (with the initial condition fixed at −100 cm).

We developed the surrogate model using a single-layer LSTM neural network with 256 hidden nodes, an input size of 9, and an output size of 1. The loss function was defined as the mean squared error (MSE) between the simulated soil water content at 0.05 m depth from the numerical model and the surrogate model. The training

Table 2
Parameter Settings of the Numerical Model

Parameters	Description	Setting
h_i	Initial condition	−100 cm
z_{lower}	Depth of soil profile	50 cm
z_{root}	Depth of Root distribution	40 cm
B_{upper}	Upper boundary condition	Atmospheric Boundary
B_{lower}	Lower boundary condition	Free Drainage
Δt_i	Initial time step	1×10^{-3} d
Δt_{min}	Minimum time step	1×10^{-5} d
Δt_{max}	Maximum time step	1 day
t_{max}	Simulation time	1095 days
ε_θ	Water content tolerance	0.001 (cm^3 cm^{-3})
ε_h	Pressure head tolerance	1 cm

procedure involved three steps: (a) generating 30,000 numerical simulations with Hydrus-1D using random parameter combinations under two baseline boundary conditions—dry (high PET, low soil moisture, LAI, and P) and wet (low PET, high soil moisture, LAI, and P); (b) splitting the data set into training (80%), validation (10%), and test (10%) subsets; and (c) considering the surrogate model acceptable when the validation MSE fell below 0.0001 cm^3 cm^{-3}. This training process was implemented using the PyTorch deep learning framework (Paszke et al., 2019).

The workflow for training the neural network–based surrogate model is illustrated in Figure S1 of Supporting Information S1. As shown in Figure S2 of Supporting Information S1, the trained surrogate model achieves performance that closely matches that of the numerical mode.

Once trained, the neural network's parameters (biases and weights) were frozen to ensure stability during the subsequent training of the SPTFs. This crucial step prevented parameter modification through backpropagation while still permitting the propagation of gradients.

2.3. Development of the Inverse Model

To evaluate the performance of the SPTF model, we employed inverse modeling as a benchmark. The parameter acquisition workflow is illustrated in Figure 3.

The input of the inverse model is the 1-year soil water content observations at the depth of 0.05 cm with a target output of the SHPs. The objective function is defined as:

$$\mathrm{MSE}(P') = \frac{1}{N}\sum_{i=1}^{N}\left[(\mathrm{SWC}_H - \mathrm{SWC}_H')^2 \times \mathrm{bLST}_i\right] \quad (17)$$

where SWC_H' represents the simulated soil water content at a depth of 0.05 m, and N denotes the total number of observation points. Model parameters P' were optimized by minimizing the MSE using the SCE-UA algorithm developed by Duan et al. (1992). The resulting optimized parameters were subsequently evaluated using an independent data set from the second year.

2.4. Comparison Between SPTFs and Conventional PTFs

To compare the performance of conventional PTFs and the proposed SPTFs in simulating soil water dynamics, we selected two PTFs developed by Zhou et al. (2025), hereafter referred to as $\mathrm{PTF_{VGM}}$ and $\mathrm{PTF_{FXW\text{-}M3}}$. These PTFs were derived using the same training data set, primarily consisting of European soils compiled by Hohenbrink et al. (2023), and identical machine learning methodologies, differing only in the underlying soil hydraulic models adopted. Both PTFs require the same set of input variables: sand, silt, and clay fractions, along with bulk density.

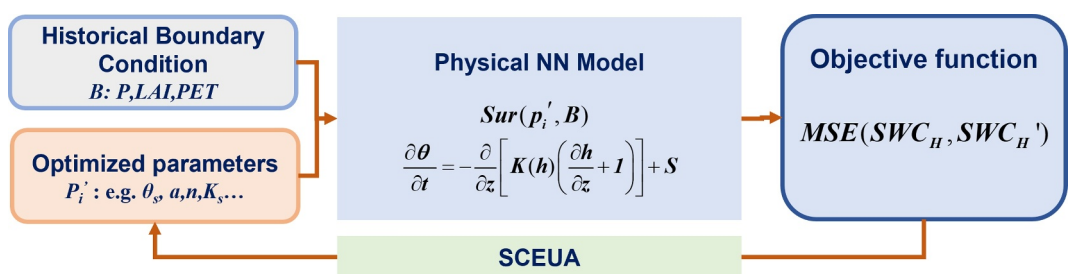

Figure 3. Framework for inverse model development. It involves four aspects: (1) the input information, (2) neural network-based surrogate model of the 1-D soil water flow model, (3) shuffled complex evolution optimization (Duan et al., 1992) algorithm (SCE-UA) and (4) objective function.

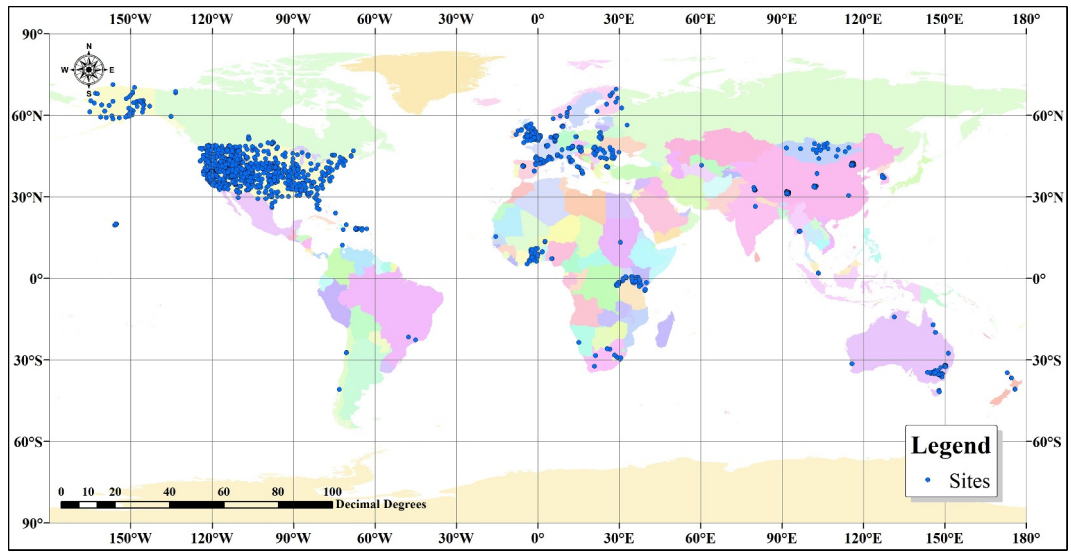

Figure 4. Spatial distribution of used sites.

To ensure a fair comparison, we selected 20 sites in Europe with measured soil properties, consistent with the regional scope of the data set used by Zhou et al. (2025). Detailed information for these sites is provided in Table S2 of Supporting Information S1.

2.5. Data

For SPTF development, we extracted all site data (from 1st January 2000 to 1st January 2024) from the International Soil Moisture Network (ISMN). Site selection adhered to two criteria: (a) a minimum of two consecutive years of soil water content observations and (b) less than 20% missing or anomalous data annually. As a result, 1,188 sites were selected, as shown in Figure 4. For continuous simulation and evaluation, missing soil water content data were filled using linear interpolation between the two nearest observations.

The 1,188 sites were randomly divided into a training set (70%, 831), validation set (15%, 178), and test set (15%, 179). The training and validation sets were used for SPTFs development, while the test set was employed to evaluate the parameter performance of SPTFs and inverse modeling. Table 3 presents a detailed summary of input data characteristics and original sources for each component.

2.6. Model Quality Metrics

The performance of the SPTFs was evaluated using two key metrics: the Root Mean Square Error (RMSE) and Nash-Sutcliffe Efficiency (NSE) between observation and prediction:

$$\mathrm{RMSE} = \sqrt{\frac{1}{N}\sum_{i=1}^{N}\left[\left(X_{\mathrm{pre},i} - X_{\mathrm{obs},i}\right)^2\right]} \tag{18}$$

$$\mathrm{NSE} = 1 - \frac{\sum_{i=1}^{N}\left[\left(X_{\mathrm{pre},i} - X_{\mathrm{obs},i}\right)^2\right]}{\sum_{i=1}^{N}\left[\left(X_{\mathrm{pre},i} - \overline{X_{\mathrm{obs},i}}\right)^2\right]} \tag{19}$$

where N is the number of data pairs; $X_{\mathrm{pre},i}$ and $X_{\mathrm{obs},i}$ are the predicted and observed soil water content at a depth of 0.05 m, respectively; $\overline{X_{\mathrm{obs},i}}$ is the mean of $X_{\mathrm{obs},i}$.

Additionally, a linear trend line ($y = ax + b$) was fitted using the least squares method, ensuring an objective assessment of the relationship between the observed and predicted data:

Table 3
Summary of the Input Data Characteristics and Their Original Sources

Data	Variables	Time range	Time resolution	Original time resolution	Source
X_H	SWC_H	1–365	Daily	Hourly	ISMN
	P_H	1–365	Daily	Daily	ERA5-Land
	LAI_H	1–365	Daily	Daily	MCD15A3H.061
	PET_H	1–365	Daily	8-day	MODIS16A2GF
	LST_H	1–365	Daily	Daily	MOD21A1D_061_LST
X_S	Sand	\	\	\	SoilGrids2.0(0–0.05 m)
	Silt	\	\	\	SoilGrids2.0(0–0.05 m)
	Clay	\	\	\	SoilGrids2.0(0–0.05 m)
	BD	\	\	\	SoilGrids2.0(0–0.05 m)
B	*P*	365–730	Daily	Daily	ERA5-Land
	LAI	365–730	Daily	Daily	MCD15A3H.061
	PET	365–730	Daily	8-day	MODIS16A2GF
	LST	365–730	Daily	Daily	MOD21A1D_061_LST
Θ_{obs}	Θ_{obs}	365–730	Daily	Hourly	ISMN

$$Q = \sum_{i=1}^{n} (X_{pre,i} - aX_{obs,i} - b)^2 \quad (20)$$

where Q is error; a and b are intercept ($cm^3\ cm^{-3}$) and slope of trend line.

To evaluate the importance of input variables for SPTF performance, we applied the permutation feature importance (FI) algorithm (Molnar, 2018). This method assumes that the trained model $F(x)$ accurately captures the nonlinear relationship between the feature matrix X and target vector Y. The process of calculating feature importance is as follows:

1. Calculate the original model error $E_{orig} = Loss(Y, F(X))$
2. For each input feature $x_i = 1, \ldots\ldots, p$ in X:
   (a) Generate feature matrix X_{perm} by shuffling x_i in X. This breaks the association between x_i and Y;
   (b) Calculate $E_{perm} = Loss(Y, F(X_{perm}))$ based on the predictions of the shuffled data;
   (c) Calculate permutation feature importance $FI_i = E_{perm}/E_{orig}$.

FI scores indicate the relative contribution of each feature x_i to model performance; higher scores denote greater importance. Conversely, FI scores below 1 suggest minimal predictive power for the corresponding feature. To mitigate the effects of inherent stochasticity in the association-breaking process, we repeated the calculation 100 times with distinct random seeds and averaged the resulting FI values to obtain a robust estimate of feature importance.

3. Results

3.1. Performance of SPTFs

Since measured SHPs were unavailable for each site, we evaluated SPTF performance by comparing simulated soil water content derived using SHPs predicted by the SPTF with observations from both training and test data sets. Figure 5 presents the simulated soil water content on 831 training and 117 test sites obtained using the SHPs estimated by the two proposed SPTFs.

Both SPTFs developed, either based on the FXW-M3 model (hereafter $SPTF_{FXW\text{-}M3}$) or the VGM model (hereafter $SPTF_{VGM}$), demonstrated good agreement between observed and simulated values on the training set (Figuress 5a and 5c), with data points clustering closely around the 1:1 line. This is evidenced by low RMSE values (0.076 $cm^3\ cm^{-3}$ for $SPTF_{FXW\text{-}M3}$ and 0.077 $cm^3\ cm^{-3}$ for $SPTF_{VGM}$) and high NSE values (0.675 and 0.658, respectively). However, the intercepts of the fitted trend lines (0.062 $cm^3\ cm^{-3}$ and 0.057 $cm^3\ cm^{-3}$)

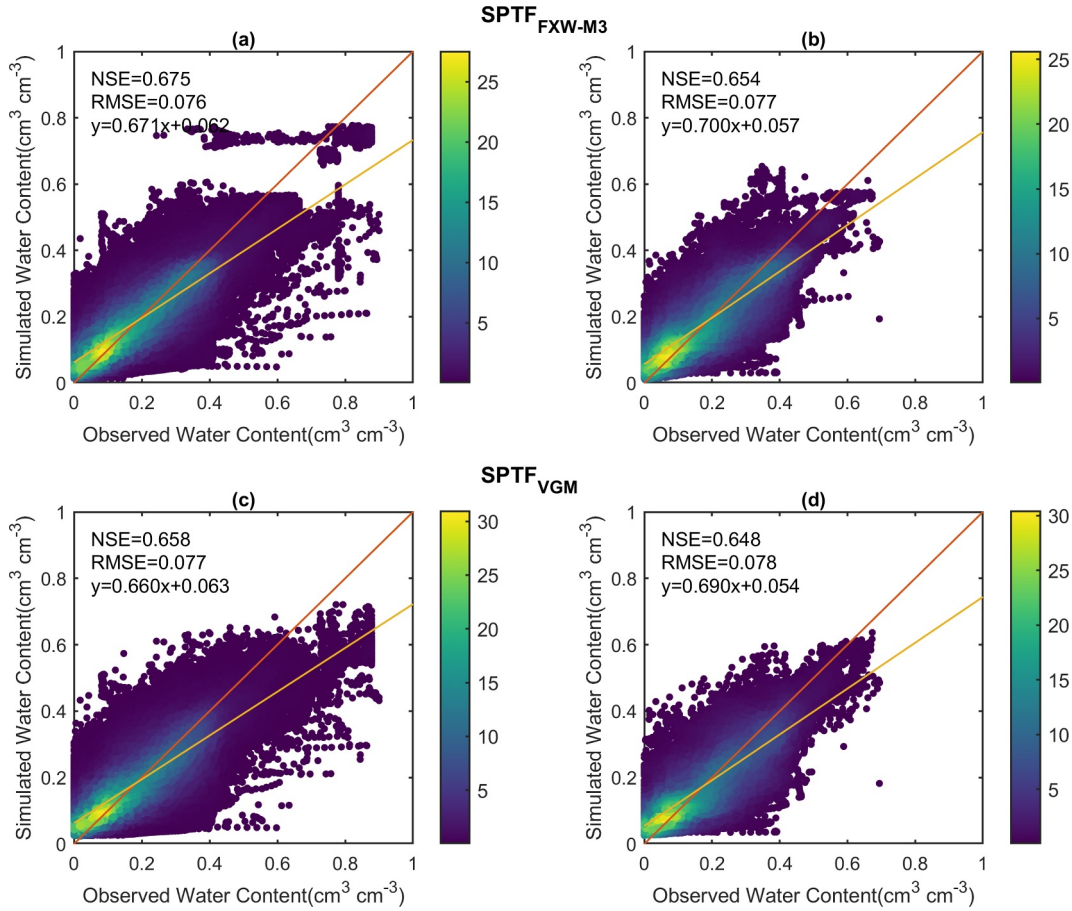

Figure 5. Performance of $SPTF_{FXW\text{-}M3}$ and $SPTF_{VGM}$ in training (a, c) and test sets (b, d). The two lines represent the 1:1 line and the fitted trend line.

suggest a slight overestimation of soil water content under drier conditions. Furthermore, slopes of the trend lines (0.671 and 0.660), being less than unity, indicate systematic underestimation at higher water contents, particularly above 0.400 $cm^3\ cm^{-3}$.

The test set results (Figures 5b and 5d) show a similar pattern, with RMSE increasing by approximately 0.01 $cm^3\ cm^{-3}$ and NSE decreasing by about 0.02 for both $SPTF_{FXW\text{-}M3}$ and $SPTF_{VGM}$, indicating consistent model performance across data sets. Consistent with the training results, both SPTFs tend to overestimate soil moisture under dry conditions and underestimate it under wet conditions.

Figure 6 further illustrates the performance of both SPTFs across different soil texture classes, land cover classes, and environmental conditions (i.e., ranges of mean soil water content and annual precipitation). Soil texture was derived from SoilGrids2.0 data (Poggio et al., 2021). Among the four dominant soil texture classes, both SPTFs achieved the best performance for clay loam (25 sites), followed by sandy loam (35 sites), loam (79 sites), and silty loam (16 sites), with mean RMSE values ranging from 0.065 to 0.092 $cm^3\ cm^{-3}$. For the remaining seven texture classes, both SPTFs showed relatively better performance for loamy sand (7 sites), sand (2 sites), clay (1 site), and sandy clay loam (5 sites), where mean RMSE values were below 0.055 $cm^3\ cm^{-3}$. In contrast, reduced performance was observed for silty clay loam (9 sites), silt (5 sites), and silty clay (1 site), with mean RMSE values between 0.072 and 0.087 $cm^3\ cm^{-3}$. A comparison between $SPTF_{FXW\text{-}M3}$ and $SPTF_{VGM}$ indicates that the two models exhibit overall similar performance, with a mean RMSE difference of less than 0.001 $cm^3\ cm^{-3}$ for five soil texture classes and being around 0.003 $cm^3\ cm^{-3}$ for the remaining six soil texture classes. However, it should be noted that soil texture classes used in this analysis were derived from SoilGrids2.0 estimates rather than direct field measurements, which may introduce additional uncertainty into this assessment.

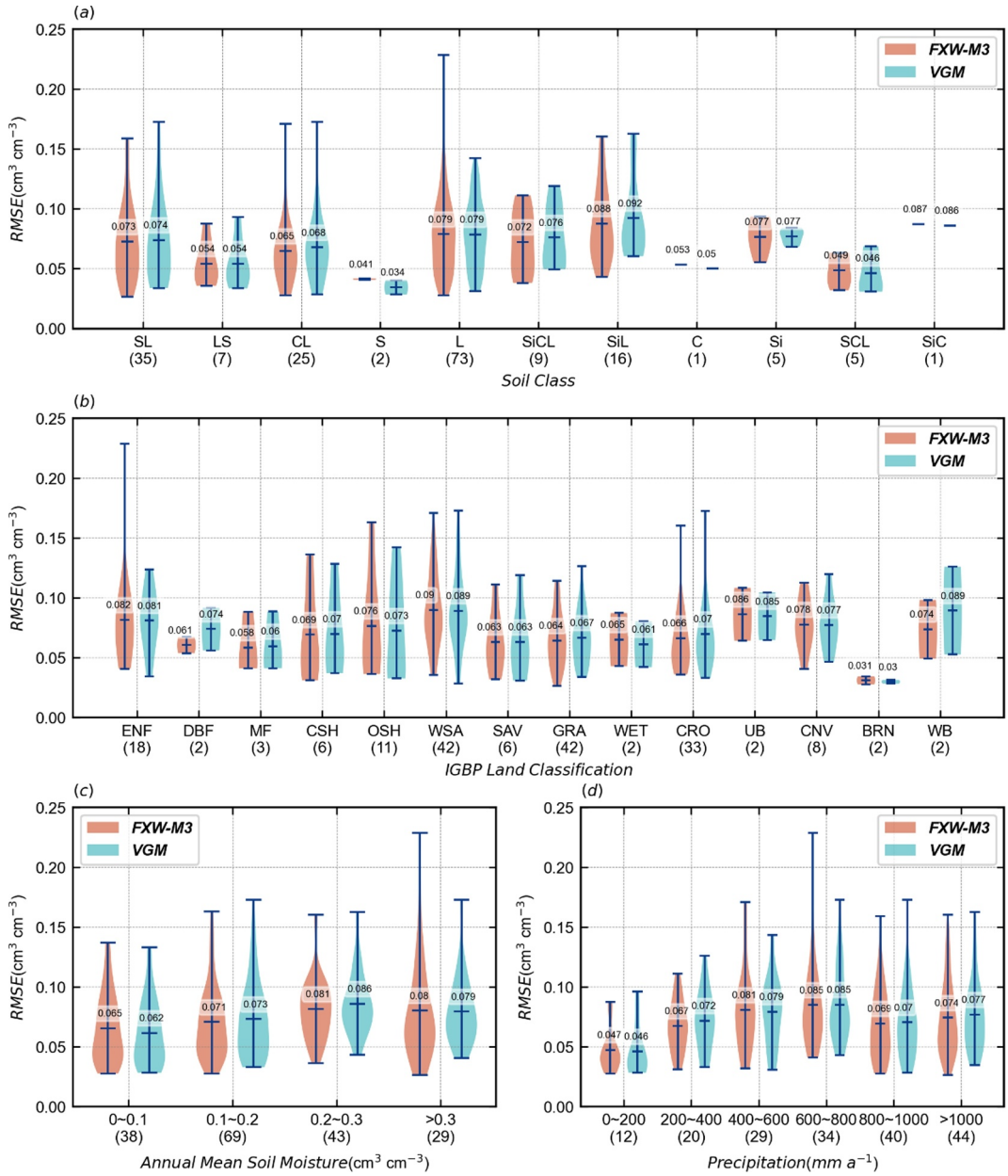

Figure 6. The performance of $SPTF_{FXW\text{-}M3}$ and $SPTF_{VGM}$ in 179 test sites, in terms of (a) different soil texture classes, (b) different International Geosphere–Biosphere Program (IGBP) ecosystem surface classification system. ENF: Evergreen needleleaf tree; DBF: Deciduous broadleaf tree; MF: Mixed forest; CSH: Closed shrubland; OSH: Open shrubland; WSA: Woody savanna; SAV: Savanna; GRA: Grassland; WET: Permanent wetland; CRO: Cropland; UB: Urban and built-up land; CNV: Cropland/natural vegetation; BRN: Barren; WB: Water Body, (c) different annual mean soil water content range and (d) different annual precipitation range. The midline in the violin plots represents the mean value.

Regarding land cover classification, for the five classes with more than 11 sites, both SPTFs perform better for grasslands (GRA, 42 sites) and croplands (CRO, 33 sites) than for woody savannas (WSA, 42 sites), open shrublands (OSH, 11 sites), and evergreen needleleaf forests (ENF, 18 sites). In the physically based soil water flow model, a uniform root depth of 40 cm is assumed for simplicity. While this assumption is reasonable for GRA and CRO, it may be less appropriate for WSA, OSH, and other land cover types characterized by deeper rooting systems. In addition, because the process-based model does not explicitly account for precipitation interception, simulation accuracy may be reduced at sites where interception plays a significant role.

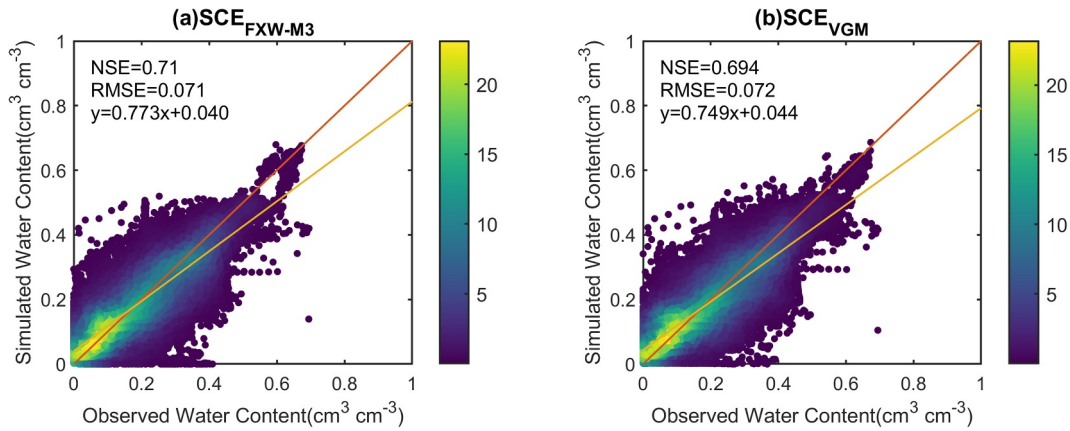

Figure 7. The performance of inverse modeling in simulating soil water content for the 179 test sites (a) FXW-M3 model and (b)VGM model between observation and simulation.

For the remaining nine land cover classes, both SPTFs report mean RMSE values exceeding 0.074 $cm^3\ cm^{-3}$ for CNV, UB, and WB, whereas mean RMSE values are below 0.070 $cm^3\ cm^{-3}$ for the other six classes. The difference between $SPTF_{FXW-M3}$ and $SPTF_{VGM}$ across land cover classifications is also very small, with mean RMSE difference being less than 0.001 $cm^3\ cm^{-3}$ for seven land cover classes and being around 0.003 $cm^3\ cm^{-3}$ for the reaming seven classes.

Performance also varied slightly with climatic and soil moisture conditions. For sites with an annual mean soil moisture below approximately 0.30 $cm^3\ cm^{-3}$ and precipitation below around 800 mm, RMSE tended to increase slightly with higher soil moisture and precipitation. Beyond these thresholds, RMSE values generally decreased. However, except for sites with mean soil moisture below 0.1 $cm^3\ cm^{-3}$ and precipitation below 200 mm, the differences were small, typically less than 0.01 $cm^3\ cm^{-3}$ across the various ranges.

In summary, the close agreement between observed and simulated values confirms the reliability of the parameters estimated by the SPTFs. Meanwhile, $SPTF_{FXW-M3}$ and $SPTF_{VGM}$ demonstrated comparable predictive performance. The minimal performance differences observed between $SPTF_{FXW-M3}$ and $SPTF_{VGM}$ could be attributed to the limited representation of these extreme moisture conditions in the observations which reduces the ability to exploit the full benefits of the FXW-M3 model.

3.2. Performance of the Inverse Model

Figure 7 illustrates the performance of the inverse model in simulating soil water content across 179 test sites, using both the FXW-M3 and VGM models. Overall, the inverse modeling approach demonstrated strong capability in capturing soil water dynamics. The two models show no obvious difference, with the FXW-M3 model showing marginally higher NSE values and steeper trendline slopes than the VGM model.

When compared to the SPTFs, inverse modeling generally achieved a better performance for both hydraulic models. Taking the FXW-M3 model as an example, inverse modeling yielded an NSE of 0.710 and an RMSE of 0.071 $cm^3\ cm^{-3}$ across the 179 test sites. In contrast, the $SPTF_{FXW-M3}$ achieved an NSE of 0.654 and an *RMS*E of 0.077 $cm^3\ cm^{-3}$. Furthermore, the trendline slope for the inverse model (Figure 7a) was 0.773, higher than that of the $SPTF_{FXW-M3}$ (0.700), while the intercept was lower (0.040 $cm^3\ cm^{-3}$ vs. 0.057 $cm^3\ cm^{-3}$), suggesting better agreement between observed and simulated values.

Figure 8 summarizes the performance of $SPTF_{FXW-M3}$ and the inverse model in simulating soil water content across 179 test sites. When stratified by soil texture class, inverse modeling generally outperformed the SPTF for all texture classes except silty clay. The performance difference is particularly pronounced for loamy sand (7 sites), sand (2 sites), silty clay loam (9 sites), silty loam (16 sites), and silt (5 sites), where inverse modeling yielded reductions in mean RMSE exceeding 0.01 $cm^3\ cm^{-3}$ relative to the SPTF.

A similar pattern is observed across land cover classifications. Inverse modeling exhibits superior performance for most land cover types, with the exception of deciduous broadleaf forest and barren land (BRN). The advantage

10.1029/2025WR041265

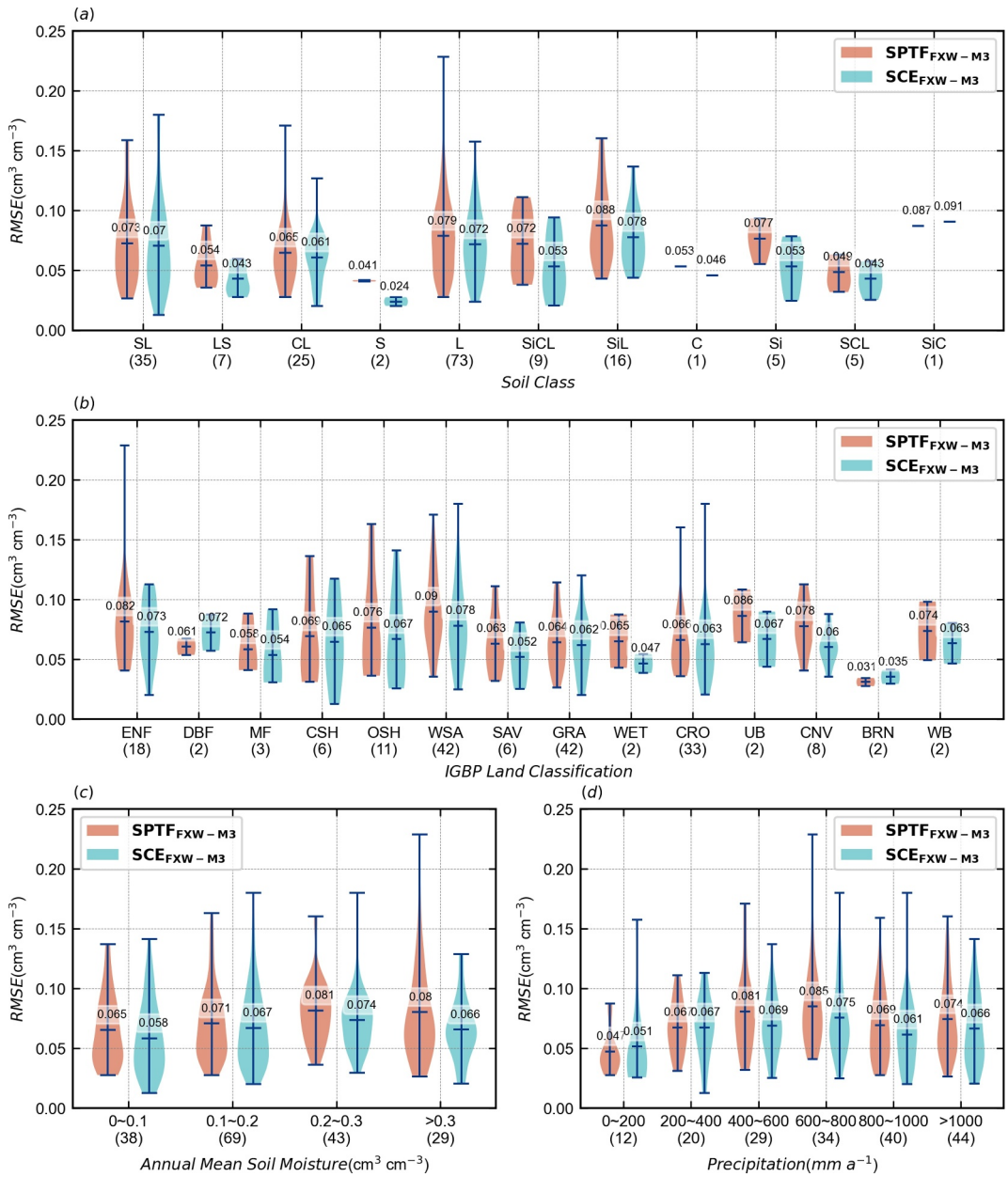

Figure 8. The performance of SPTF$_{FXW-M3}$ and inverse modeling in simulating soil water content for 179 test sites, in terms of (a) different soil texture classes, (b) different International Geosphere–Biosphere Program (IGBP) ecosystem surface classification system. (c) Different annual mean soil water content range and (d) different annual precipitation range. The midline in the violin plots represents the mean value.

of inverse modeling is most evident for woody savannas (WSA, 42 sites), savannas (SAV, 6 sites), wetlands (WET, 2 sites), urban areas (UB, 2 sites), cropland/natural vegetation mosaics (CNV, 8 sites), and water bodies (WB, 2 sites), where mean RMSE values are more than 0.01 cm^3 cm^{-3} lower than those obtained with the SPTF. Notably, the largest degradation in SPTF performance tends to occur for soil texture and land cover classes with relatively small sample sizes.

When grouped by climatic and soil moisture conditions, the reduced performance of the SPTF is most pronounced at high soil moisture levels (>0.3 cm^3 cm^{-3}) and under intermediate annual precipitation regimes (400–800 mm).

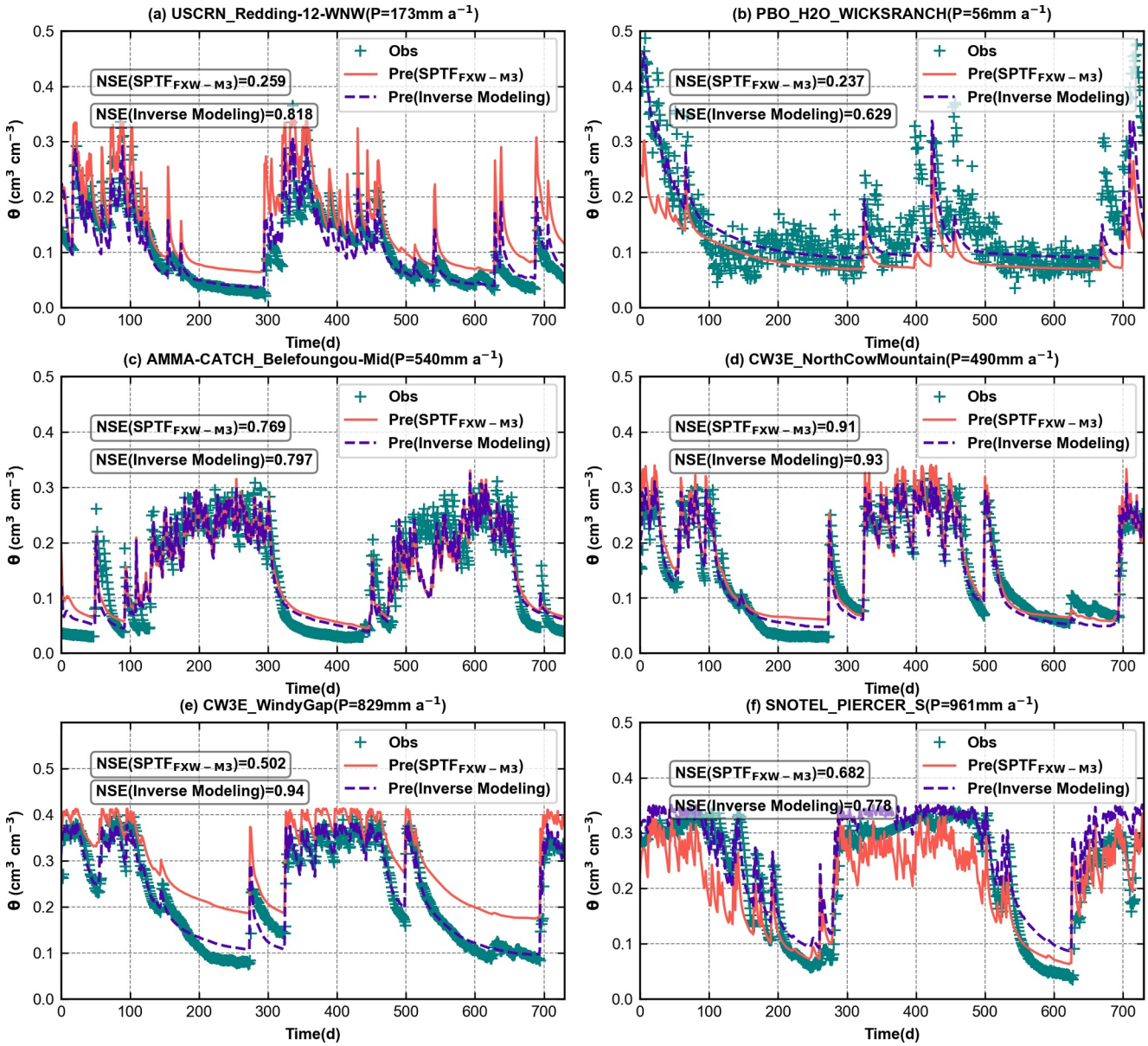

Figure 9. The performance of inverse model and SPTF$_{FXW-M3}$ in simulating soil water content for (a) site USCRN_Redding-12-WNW with mean annual precipitation of 173 mm, (b) site PBO_H2O_WICKSRANCH with mean annual precipitation of 56 mm, (c) site AMMA-CATCH_Belefoungou-Mid with mean annual precipitation of 540 mm, (d) site CW3E_NorthCowMountain with mean annual precipitation of 490 mm, (e) site CW3E_WindyGap with mean annual precipitation of 829 mm and (f) site SNOTEL_PIERCER_S with mean annual precipitation of 961 mm.

Figure 9 illustrates simulated soil moisture dynamics at six representative sites spanning a range of rainfall conditions. At these sites, SPTFs show larger deviations from observations under both very wet (Figures 9b, 9e, and 9f) and very dry (Figures 9a and 9e) conditions, resulting in substantially lower accuracy compared to inverse modeling.

Overall, SPTFs exhibit reduced performance relative to inverse modeling, particularly for soil texture and land cover classes with limited sample sizes and under extremely wet or dry soil moisture conditions. This discrepancy can be attributed to differences in their optimization strategies: inverse modeling was calibrated on a site-by-site basis using site-specific loss functions, whereas SPTFs were trained against observations aggregated from all 831 training sites. As most observations fall within an intermediate soil moisture range, SPTFs achieve higher accuracy under typical conditions, but exhibit diminished performance at the extremes. Thus, there is a need for

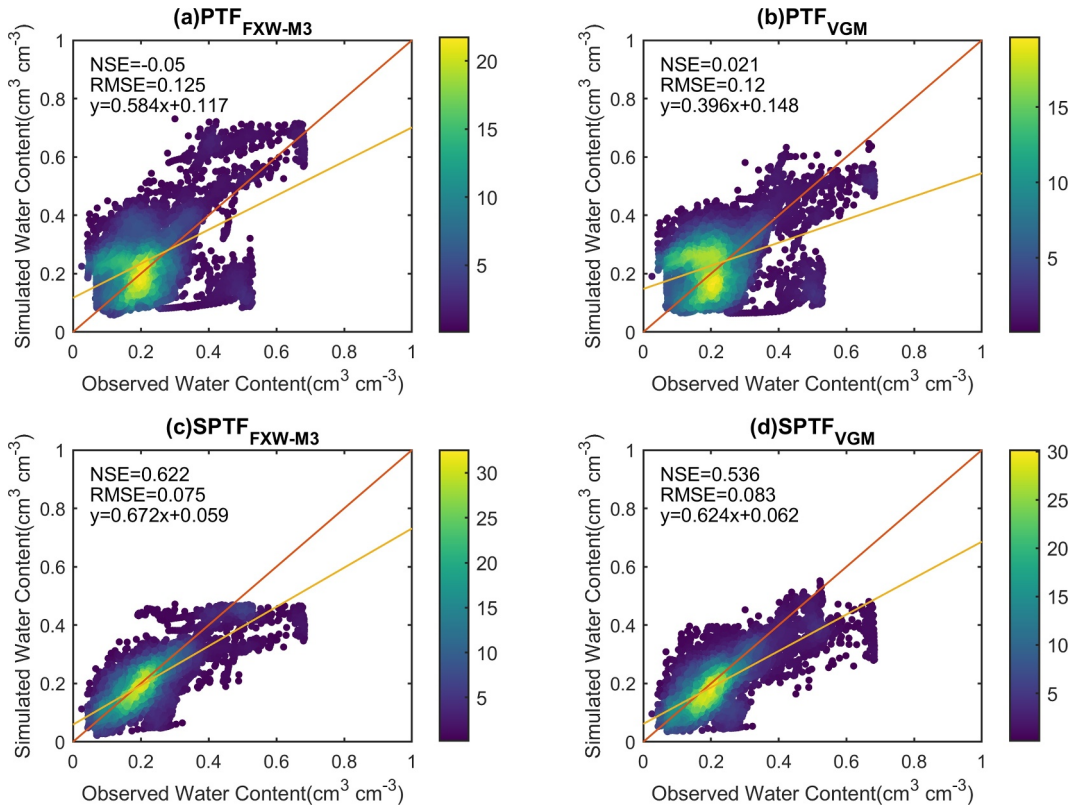

Figure 10. The performance comparison of $PTF_{FXW\text{-}M3}$ (a), PTF_{VGM} (b), $SPTF_{FXW\text{-}M3}$ (c), $SPTF_{VGM}$ (d) between observation and simulation. The detailed information about $PTF_{FXW\text{-}M3}$ and PTF_{VGM} can be found in Zhou et al. (2025).

further improving SPTF performance under very low and very high soil moisture conditions, for example, by assigning greater weights to extreme observations in the loss function.

3.3. Performance of Conventional PTFs

Figure 10 presents the simulation results of soil water dynamics at 20 evaluation sites, comparing two traditional PTFs and two SPTFs. Although the 20 sites have measured input data and are located within the same geographical region used to develop the two traditional PTFs, both PTFs exhibited poor performance in reproducing the observed soil water content dynamics. Specifically, the NSE values were −0.050 and 0.021, and the RMSE values were 0.125 and 0.120 $cm^3\ cm^{-3}$ for $PTF_{FXW\text{-}M3}$ and PTF_{VGM}, respectively. Meanwhile, the $PTF_{FXW\text{-}M3}$ slightly outperformed PTF_{VGM} in both dry and wet ends, as indicated by a higher slope and lower intercept of the regression trend line.

In contrast, the proposed SPTFs showed substantially improved performance in modeling soil water dynamics. For $SPTF_{FXW\text{-}M3}$, the NSE reached 0.622 with an RMSE of 0.075 $cm^3\ cm^{-3}$, while $SPTF_{VGM}$ achieved an NSE of 0.536 and an RMSE of 0.083 $cm^3\ cm^{-3}$. Nevertheless, both SPTFs tended to underestimate soil water content when observed values exceeded approximately 0.40 $cm^3\ cm^{-3}$, as reflected by relatively low trendline slopes of 0.672 and 0.624 for $SPTF_{FXW\text{-}M3}$ and $SPTF_{VGM}$, respectively. Overall, $SPTF_{FXW\text{-}M3}$ outperformed $SPTF_{VGM}$ across the 20 evaluation sites using measured soil texture data.

We also present in Figure S4 of Supporting Information S1 the performance of the two PTFs using soil texture inputs from SoilGrids2.0 (Poggio et al., 2021). As shown, PTFs with estimated soil texture information exhibit slightly poorer performance than those using measured soil texture data.

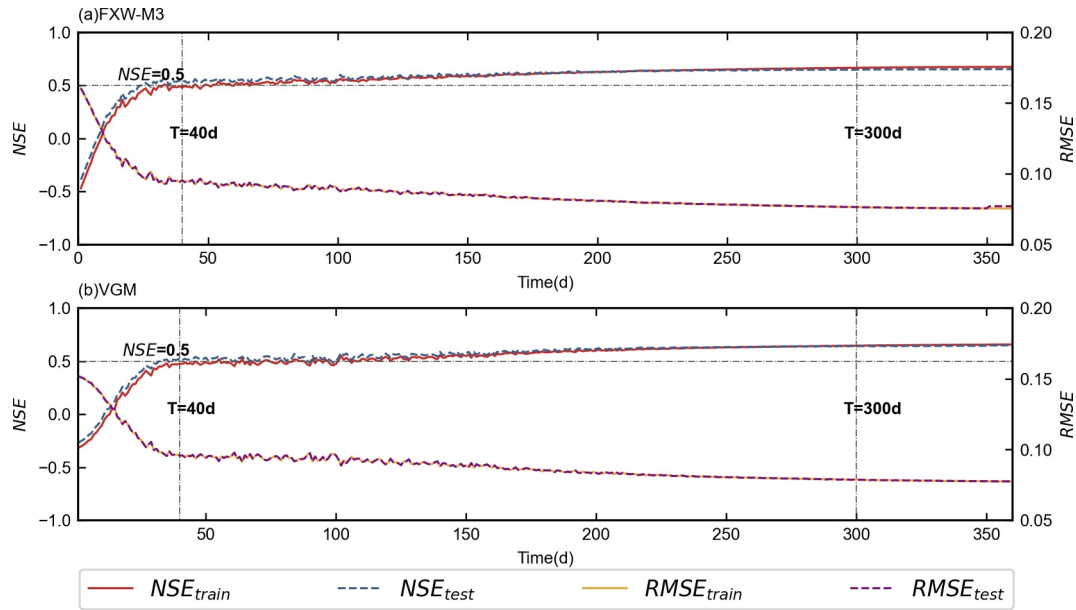

Figure 11. The Nash-Sutcliffe Efficiency and Root Mean Square Error for varying length input of time-series data. (a) The $SPTF_{FXW\text{-}M3}$; (b) the $SPTF_{VGM}$.

3.4. Impact of Input Length on SPTFs Performance

The previous evaluation (Figure 5) employed a 365-day time series of soil water content observations as input for the SPTF. However, acquiring such long-term observational data can be challenging. To address this issue, we investigated the sensitivity of SPTF performance to varying input lengths.

Figure 11 illustrates how RMSE and NSE values for both the training and test sets vary with the temporal length of input data. To ensure the robustness of this analysis, 10 random sub-sequences of observation periods shorter than 350 days were selected, and the corresponding RMSE and NSE values were averaged across the 10 iterations.

For both SPTFs, the NSE demonstrated distinct trends as a function of time-series length. During the initial period (up to approximately 40 days), NSE increased rapidly toward 0.5. Subsequently, between 40 and roughly 180 days, it rose slowly with marked fluctuations. Beyond this interval, NSE increased steadily and stabilized with minimal variation, eventually converging to the values achieved using the full 365-day input series. Similarly, RMSE followed similar patterns with time series length as NSE, but exhibited an inverse relationship.

Overall, the results indicate that a minimum temporal input length of approximately 40 days is required to achieve NSE values exceeding 0.5 in both training and testing. Below this threshold, model performance deteriorates significantly.

3.5. Importance of Input Variables on SPTFs Performance

Figure 12 illustrates the relative importance of input variables in determining SPTF performance, assessed via FI scores. In simple terms, the FI score of a given factor represents the ratio between the Loss values calculated without and with the correct inclusion of that factor. Higher FI values denote a stronger influence on the model output, while values close to one indicate negligible impact.

Across both the training and test data sets, the historical soil water content (SWC_H) consistently yielded the highest FI scores (exceeding 3), whereas all other variables showed FI scores near 1.0, underscoring the dominant role of SWC_H. This emphasizes the dominant role of SWC_H in driving model performance. Despite slight variations in FI values between the training and test sets, the ranking of input importance remains consistent: SWC_H ranks highest, followed by LAI_H, P_H and PET_H, with the remaining variables contributing marginally.

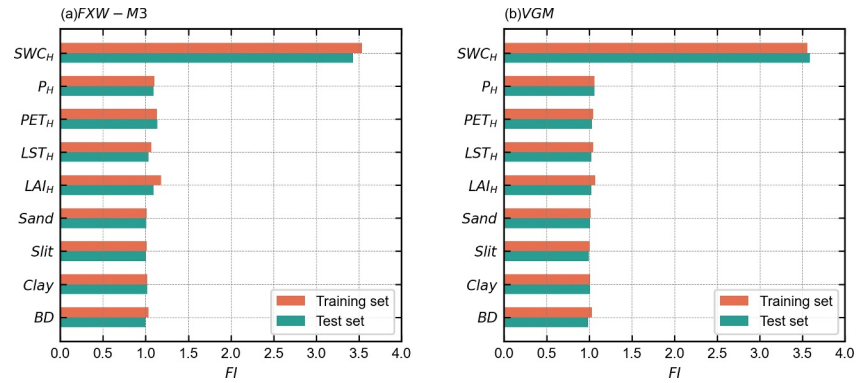

Figure 12. The FI scores for features in SPTFs. The higher the FI score, the more importance of the variable to the model performance.

Notably, the much lower FI scores (around 1) associated with soil texture information can be attributed to two main factors. First, soil texture variables are derived from SoilGrids2.0 (Poggio et al., 2021) and therefore represent gridded estimates rather than site-specific measurements. Second, the spatial scale of the study sites does not match the 1 km resolution of SoilGrids2.0. Together, these factors likely limit the contribution of soil texture information within the SPTF framework. For a more reliable assessment of variable importance, future work should develop SPTFs using measured soil texture data.

Given the critical influence of SWC_H, we further evaluated SPTF performance using SWC_H as the sole input, with results presented in Figure S3 of Supporting Information S1. As expected, performance declined compared to models using the full suite of input variables, yet both SPTFs still effectively captured soil water dynamics. For the test set, NSE values were 0.589 and 0.613, and RMSE values were 0.084 and 0.081 $cm^3\ cm^{-3}$ for the $SPTF_{FXW\text{-}M3}$ and $SPTF_{VGM}$, respectively.

4. Discussion

4.1. Comparison Between SPTF and Inverse Modeling

While both SPTFs and inverse models serve the purpose of estimating SHPs, they differ fundamentally in their structure and implementation. The SPTFs, akin to traditional PTFs, are data-driven models trained on a historical data set. Once trained, they enable rapid prediction of SHPs from readily available input variables, without the need to run a physically based soil water flow model at each application site.

In contrast, inverse modeling operates on a site-specific basis. For each site, a forward process model must be defined and repeatedly executed to iteratively optimize parameters. These issues can result in failure to retrieve valid parameters. Although recent advances such as neural operator-based surrogate modeling (e.g., Guo et al., 2024; Taccari et al., 2024) have sought to improve efficiency, they do not fully resolve these limitations.

For example, generating the results shown in Figure 7 via inverse modeling required more than 2 hrs of computation, while the results in Figure 5, derived from SPTFs, were obtained almost instantaneously. From a practical perspective, this stark contrast underscores the substantially higher computational efficiency and operational simplicity of SPTFs for large-scale or repeated applications.

Furthermore, inverse modeling directly optimizes parameters for each individual site and thus benefits from localized fitting, which naturally yields better performance. In contrast, SPTFs must generalize across diverse sites, learning the complex functional relationships between input variables and SHPs during training. This additional layer of abstraction, approximating parameters based on learned patterns, explains why SPTF performance, while robust, may not always match the site-specific accuracy achieved by inverse modeling.

4.2. The Differences Between SPTF and Conventional PTF

While both the proposed SPTFs and conventional PTFs can directly estimate SHPs from input data, they differ fundamentally in their input requirements, training methodology, and prediction targets. Traditional PTFs

typically rely on static soil properties such as texture and bulk density (e.g., Schaap et al., 2001; Wang et al., 2022; Zhang & Schaap, 2017). In contrast, SPTFs are designed to leverage dynamic information, with historical soil water content observations serving as the most influential input.

In terms of training approaches, PTFs are commonly developed using machine learning algorithms such as random forests (Breiman, 2001), whereas SPTFs utilize deep learning architectures, such as LSTM networks, to learn the mapping from dynamic inputs to SHPs. Regarding prediction targets, traditional PTFs aim to reproduce SHPs derived from fitting models (e.g., VGM or FXW-M3) to measured properties obtained from relatively small soil samples (Minasny et al., 2024; Rudiyanto et al., 2021; Wang et al., 2022; Zhang & Schaap, 2017; Zhou et al., 2025). As such, the output parameters are assumed to represent intrinsic (albeit model-dependent) soil properties. In contrast, SPTFs estimate *effective* SHPs optimized for a specific process-based model—in this study, a one-dimensional soil water flow model governed by the Richardson–Richards equation. These parameters are thus tailored to reproduce observed soil water dynamics within the context of the underlying model structure and its governing assumptions.

An evaluation across 20 sites with measured soil texture data revealed that the hydraulic parameters predicted by the two traditional PTFs failed to adequately reproduce observed soil water content dynamics when implemented in the 1-D Richardson–Richards equation model. This result aligns with prior findings (Chirico et al., 2010; Paschalis et al., 2022; Vereecken et al., 1992; Weihermuller et al., 2021), which reported that traditional PTFs often perform poorly in simulating soil water fluxes and related processes. Two primary factors may explain the limited field applicability of traditional PTFs: (a) hydraulic properties derived from small-scale laboratory samples often do not capture the spatial heterogeneity characteristic of field conditions (e.g., Rudiyanto et al., 2021; Schaap et al., 2001; Schaap & Leij, 1998; Wang et al., 2022; Zhang & Schaap, 2017), and (b) static input variables, such as texture and bulk density, may lack sufficient information to characterize the dynamic behavior of hydrological systems (Van Looy et al., 2017; Vereecken et al., 2010; Weber et al., 2024).

In contrast, the SPTFs produce parameter estimates that are inherently better suited to field-scale hydrological modeling, as they are directly conditioned on observed water dynamics. However, as discussed in Section 4.1, these estimates are not universally transferable; they are intrinsically dependent on the process-based model employed and the validity of its structural and physical assumptions. Nevertheless, the proposed SPTFs rely on in situ soil water content historical data, which may be difficult and costly to obtain. This reliance makes their application more expensive than that of traditional PTFs. Therefore, further research is needed to enhance the applicability of SPTFs, for example, by incorporating satellite-based soil water content products as inputs.

4.3. Evaluation of FXW-M3 and VGM Models in Site-Scale

Although the FXW-M3 model, which accounts for film flow, capillarity, and soil structural effects, has demonstrated significantly better performance than the capillarity-based VGM model in characterizing soil hydraulic properties (Wang et al., 2023, 2025) and in the development of traditional PTFs (Zhou et al., 2025), both models yielded comparable performance when implemented within the SPTFs (Figures 5b and 5d) and in inverse modeling (Figures 7a and 7b) for simulating soil water dynamics at field sites. A recent study by Şahin and Gündüz (2025) also reported that the FXW model proposed by Wang et al. (2018), which accounts for capillarity and film flow and represents an early version of the FXW-M3 model, performed slightly better than the VGM model in inverse modeling when tested with ISMN data.

The comparable performance between the FXW-M3 and VGM models can be attributed to two main factors. First, the majority of observed soil water content values were concentrated in the moderate range, with relatively few observations under very wet or very dry conditions. Notably, the advantages of the FXW-M3 model over the VGM model lie in its ability to account for additional soil structural effects, which become significant under near-saturated conditions (Børgesen et al., 2006; Larsbo et al., 2005; Schaap & Genuchten, 2006; Wang et al., 2023), and adsorption forces, which are particularly important at low water content (Arthur et al., 2013; Resurreccion et al., 2011; Schaap & Leij, 2000; Tuller et al., 1999; Tuller & Or, 2005; Wang et al., 2013, 2016, 2018). As a result, the limited representation of these extreme moisture conditions in the observations reduces the ability to exploit the full benefits of the FXW-M3 model. This explains the minimal performance differences observed between $SPTF_{FXW\text{-}M3}$ and $SPTF_{VGM}$, as well as between the inverse modeling results based on the two models, in simulating soil water content dynamics in this study.

4.4. Limitations in the SPTFs Development

While the proposed SPTFs demonstrated strong performance in estimating effective SHPs suitable for field-scale applications, they are subject to three key limitations.

First, as extensively discussed in the previous section, the estimated parameters from the SPTFs are *effective* rather than *measured* SHPs, and are inherently dependent on the underlying physical model. Therefore, the SPTFs developed in this study may not be directly applicable to other models with different representations of soil water flow processes than the Richards Equation-based framework. Nonetheless, given the flexible nature of the framework, one could readily retrain a specific SPTF tailored to a different physical model. To improve the ability of SPTFs to estimate physically meaningful SHPs, one promising direction is to incorporate more accurate and comprehensive process-based models, along with the use of dual types of observations (e.g., soil water content at different depths and ET data) to constrain the training. Another approach is to include in situ measurements of SHPs under field conditions to further constrain the parameter learning process.

Second, limitations arise from data availability and quality. In this study, most sites meeting the selection criteria are located in the United States and Europe. This geographic bias limits the generalizability of the SPTFs, particularly for underrepresented regions such as tropical Africa, where ISMN data are sparse (O & Orth, 2021). Furthermore, the majority of observed soil water content data fall within the medium-to-low moisture range, suggesting limited reliability in predicting SHPs under near-saturated or highly humid conditions. In addition, inconsistencies in spatial and temporal resolution among different data sources introduce substantial uncertainty, as shown in prior studies (Li et al., 2024; Patil et al., 2011; Pogson et al., 2015; Zheng et al., 2018). Future work should explicitly account for these variations to improve the robustness and transferability of SPTF predictions.

Third, the proposed SPTFs are heavily dependent on in situ soil historical water content data, which are often difficult and costly to obtain. In contrast, the contributions from other time-series and static data are markedly smaller. Further research is needed to assess whether comparable predictive performance can be achieved using more readily accessible data sources, such as satellite-based soil water content products.

5. Conclusions

In this study, we developed new Site-Specific Pedotransfer Functions (SPTFs) using a dynamic Physical Learning (dPL) framework to predict high-performance SHPs. This approach integrates dynamic input (e.g., soil water content time series) with static soil attributes, coupling deep learning with physically based modeling to enhance parameter compatibility with process models.

Evaluation across diverse sites demonstrates that SPTFs achieve comparable performance to inverse modeling while maintaining prediction efficiency similar to traditional PTFs. This effectively bridges the gap between conventional PTFs and the estimation of model-compatible parameters. The results highlight the promising potential of SPTFs for land surface modeling and broader hydrological applications. Moreover, this work underscores the utility of deep learning frameworks in improving both the accuracy and practicality of parameter estimation (Shen et al., 2023).

Nevertheless, SPTFs still have some limitations, such as their inability to predict true measured SHPs and their reliance on soil water content time series. These challenges call for further research to enhance the generalizability and practical applicability of SPTFs across diverse models and environmental conditions.

Conflict of Interest

The authors declare no conflicts of interest relevant to this study.

Data Availability Statement

The ISMN site data can be download from https://ismn.earth/en/dataviewer. The LST(MOD21A1D_061_LST), PET (MODIS16A2GF), Precipitation (ERA5-Land) and LAI (MCD15A3H.061) can be download from https://code.earthengine.google.com. The SoilGrids v2.0 data can be accessed via http://doi.org/10.5194/soil-7-217-2021.

The code for the developed SPTFs and the surrogate model can be found at https://doi.org/10.6084/m9.figshare.29835380.v2. A user-friendly interface is also provided for users to apply the SPTFs (https://cug-wang.streamlit.app/).

Acknowledgments
This research was supported in part by the National Natural Science Foundation of China (Grants 42425207; U2244230; 42071045) and in part by the Natural Science Foundation of Hubei (No. 2024AFD376) and in part by Fundamental and Interdisciplinary Disciplines Breakthrough Plan of the Ministry of Education of China (No. JYB2025XDXM911).

References

Arthur, E., Tuller, M., Moldrup, P., Resurreccion, A. C., Meding, M. S., Kawamoto, K., et al. (2013). Soil specific surface area and non-singularity of soil-water retention at low saturations. *Soil Science Society of America Journal*, *77*(1), 43–53. https://doi.org/10.2136/sssaj2012.0262

Bandai, T., & Ghezzehei, T. A. (2021). Physics-Informed neural networks with monotonicity constraints for richardson-richards equation: Estimation of constitutive relationships and soil water flux density from volumetric water content measurements. *Water Resources Research*, *57*(2), e2020WR027642. https://doi.org/10.1029/2020wr027642

Bandai, T., & Ghezzehei, T. A. (2022). Forward and inverse modeling of water flow in unsaturated soils with discontinuous hydraulic conductivities using physics-informed neural networks with domain decomposition. *Hydrology and Earth System Sciences*, *26*(16), 4469–4495. https://doi.org/10.5194/hess-26-4469-2022

Baroni, G., Facchi, A., Gandolfi, C., Ortuani, B., Horeschi, D., & van Dam, J. C. (2010). Uncertainty in the determination of soil hydraulic parameters and its influence on the performance of two hydrological models of different complexity. *Hydrology and Earth System Sciences*, *14*(2), 251–270. https://doi.org/10.5194/hess-14-251-2010

Borgesen, C. D., Iversen, B. V., Jacobsen, O. H., & Schaap, M. G. (2008). Pedotransfer functions estimating soil hydraulic properties using different soil parameters. *Hydrological Processes*, *22*(11), 1630–1639. https://doi.org/10.1002/hyp.6731

Børgesen, C. D., Jacobsen, O. H., Hansen, S., & Schaap, M. G. (2006). Soil hydraulic properties near saturation, an improved conductivity model. *Journal of Hydrology*, *324*(1–4), 40–50. https://doi.org/10.1016/j.jhydrol.2005.09.014

Borgesen, C. D., & Schaap, M. G. (2005). Point and parameter pedotransfer functions for water retention predictions for Danish soils. *Geoderma*, *127*(1–2), 154–167. https://doi.org/10.1016/j.geoderma.2004.11.025

Bouma, J. (1989). Using soil survey data for quantitative land evaluation. *Advances in Soil Sciences*, *9*, 177–213. https://doi.org/10.1007/978-1-4612-3532-3_4

Breiman, L. (2001). Random forests. *Machine Learning*, *45*(1), 5–32. https://doi.org/10.1023/a:1010933404324

Chirico, G. B., Medina, H., & Romano, N. (2010). Functional evaluation of PTF prediction uncertainty: An application at hillslope scale. *Geoderma*, *155*(3–4), 193–202. https://doi.org/10.1016/j.geoderma.2009.06.008

Dai, Y. J., Xin, Q. C., Wei, N., Zhang, Y. G., Wei, S. G., Yuan, H., et al. (2019). A global high-resolution data set of soil hydraulic and thermal properties for land surface modeling. *Journal of Advances in Modeling Earth Systems*, *11*(9), 2996–3023. https://doi.org/10.1029/2019ms001784

Duan, Q. Y., Sorooshian, S., & Gupta, V. (1992). Effective and efficient global optimization for conceptual rainfall-runoff models. *Water Resources Research*, *28*(4), 1015–1031. https://doi.org/10.1029/91wr02985

Fatichi, S., Or, D., Walko, R., Vereecken, H., Young, M. H., Ghezzehei, T. A., et al. (2020). Soil structure is an important omission in Earth System Models. *Nature Communications*, *11*(1), 522. https://doi.org/10.1038/s41467-020-14411-z

Fredlund, D. G., & Xing, A. Q. (1994). Equations for the soil-water characteristic curve. *Canadian Geotechnical Journal*, *31*(4), 521–532. https://doi.org/10.1139/t94-061

Guo, Q., He, Y., Liu, M., Zhao, Y., Liu, Y. Z., & Luo, J. (2024). Reduced geostatistical approach with a fourier neural operator surrogate model for inverse modeling of hydraulic tomography. *Water Resources Research*, *60*(6), e2023WR034939. https://doi.org/10.1029/2023wr034939

Hochreiter, S., & Schmidhuber, J. (1997). Long short-term memory. *Neural Computation*, *9*(8), 1735–1780. https://doi.org/10.1162/neco.1997.9.8.1735

Hoffman, G. J., & Van Genuchten, M. T. (1983). Soil properties and efficient water use: Water management for salinity control. *Limitations to efficient water use in crop production*, 73–85. https://doi.org/10.2134/1983.limitationstoefficientwateruse.c5

Hohenbrink, T. L., Jackisch, C., Durner, W., Germer, K., Iden, S. C., Kreiselmeier, J., et al. (2023). Soil water retention and hydraulic conductivity measured in a wide saturation range. *Earth System Science Data*, *15*(10), 4417–4432. https://doi.org/10.5194/essd-15-4417-2023

Kraft, B., Jung, M., Körner, M., Koirala, S., & Reichstein, M. (2022). Towards hybrid modeling of the global hydrological cycle. *Hydrology and Earth System Sciences*, *26*(6), 1579–1614. https://doi.org/10.5194/hess-26-1579-2022

Lamorski, K., Pachepsky, Y., Slawihski, C., & Walczak, R. T. (2008). Using Support Vector Machines to develop pedotransfer functions for water retention of soils in Poland. *Soil Science Society of America Journal*, *72*(5), 1243–1247. https://doi.org/10.2136/sssaj2007.0280N

Larsbo, M., Roulier, S., Stenemo, F., Kasteel, R., & Jarvis, N. (2005). An improved dual-permeability model of water flow and solute transport in the vadose zone. *Vadose Zone Journal*, *4*(2), 398–406. https://doi.org/10.2136/vzj2004.0137

Li, P. J., Zha, Y. Y., Zhang, Y. G., Tso, C. H. M., Attinger, S., Samaniego, L., & Peng, J. (2024). Deep learning integrating Scale conversion and Pedo-Transfer function to avoid potential errors in cross-scale transfer. *Water Resources Research*, *60*(3), e2023WR035543. https://doi.org/10.1029/2023wr035543

Liang, X., Lettenmaier, D. P., Wood, E. F., & Burges, S. J. (1994). A simple hydrologically based model of land surface water and energy fluxes for general circulation models. *Journal of Geophysical Research*, *99*(D7), 14415–14428. https://doi.org/10.1029/94jd00483

Minasny, B., Bandai, T., Ghezzehei, T. A., Huang, Y.-C., Ma, Y., McBratney, A. B., et al. (2024). Soil science-informed machine learning. *Geoderma*, *452*, 117094. https://doi.org/10.1016/j.geoderma.2024.117094

Molnar, C. (2018). A guide for making black box models explainable, *2*(3), 10. https://christophm.github.io/interpretable-ml-book

Mualem, Y. (1976). A new model for predicting the hydraulic conductivity of unsaturated porous media. *Water Resources Research*, *12*(3), 513–522. https://doi.org/10.1029/WR012i003p00513

Nasta, P., Szab, B., & Romano, N. (2021). Evaluation of pedotransfer functions for predicting soil hydraulic properties: A voyage from regional to field scales across Europe. *Journal of Hydrology-Regional Studies*, *37*, 100903. https://doi.org/10.1016/j.ejrh.2021.100903

Neuman, S. P., Feddes, R. A., & Bresler, E. (1974). Finite element simulation of flow in saturated - Unsaturated soils considering water uptake by plants.

O, S., & Orth, R. (2021). Global soil moisture data derived through machine learning trained with in-situ measurements. *Scientific Data*, *8*(1), 170. https://doi.org/10.1038/s41597-021-00964-1

Paschalis, A., Bonetti, S., Guo, Y. R., & Fatichi, S. (2022). On the uncertainty induced by pedotransfer functions in terrestrial biosphere modeling. *Water Resources Research*, *58*(9), e2021WR031871. https://doi.org/10.1029/2021wr031871

Paszke, A., Gross, S., Massa, F., Lerer, A., Bradbury, J., Chanan, G., et al. (2019). PyTorch: An imperative style, high-performance deep learning Library. In *Paper presented at the 33rd conference on neural information processing systems (NeurIPS)*. CANADA.

Patil, A., Deng, Z. Q., & Malone, R. F. (2011). Input data resolution-induced uncertainty in watershed modelling. *Hydrological Processes*, *25*(14), 2302–2312. https://doi.org/10.1002/hyp.8018

Poggio, L., de Sousa, L. M., Batjes, N. H., Heuvelink, G. B. M., Kempen, B., Ribeiro, E., & Rossiter, D. (2021). SoilGrids 2.0: Producing soil information for the globe with quantified spatial uncertainty. *Soils*, *7*(1), 217–240. https://doi.org/10.5194/soil-7-217-2021

Pogson, M., Smith, P. J. E. M., & Software. (2015). Effect of spatial data resolution on uncertainty. *63*, 87–96.

Rawls, W. J., & Brakensiek, D. L. (1982). Estimating soil-water retention from soil properties. *Journal of the Irrigation and Drainage Division-Asce*, *108*(2), 166–171. https://doi.org/10.1061/jrcea4.0001383

Resurreccion, A. C., Moldrup, P., Tuller, M., Ferré, T. P. A., Kawamoto, K., Komatsu, T., & Jonge, L. W. (2011). Relationship between specific surface area and the dry end of the water retention curve for soils with varying clay and organic carbon contents. *Water Resources Research*, *47*(6). https://doi.org/10.1029/2010wr010229

Richards, L. A. (1931). Capillary conduction of liquids through porous mediums. *Physics*, *1*(5), 318–333. https://doi.org/10.1063/1.1745010

Richardson, L. F. (1922). Weather prediction by numerical process. Franklin Classics.

Ritchie, J. T. (1972). Model for predicting evaporation from a row crop with incomplete cover. *Water Resources Research*, *8*(5), 1204–1213. https://doi.org/10.1029/WR008i005p01204

Rudiyanto, Minasny, B., Chaney, N. W., Maggi, F., Giap, S. G. E., Shah, R. M., et al. (2021). Pedotransfer functions for estimating soil hydraulic properties from saturation to dryness. *Geoderma*, *403*, 115194. https://doi.org/10.1016/j.geoderma.2021.115194

Şahin, O. G., & Gündüz, O. (2025). Derivation of soil hydraulic properties (SHPs) using a Physics-Based inverse calibration method and international soil moisture network database. *Journal of Hydrology*, *660*, 133445. https://doi.org/10.1016/j.jhydrol.2025.133445

Schaap, M. G., & Genuchten, M. T. (2006). A modified Mualem–van Genuchten formulation for improved description of the hydraulic conductivity near saturation. *Vadose Zone Journal*, *5*(1), 27–34-27–34.

Schaap, M. G., & Leij, F. J. (1998). Using neural networks to predict soil water retention and soil hydraulic conductivity. *Soil and Tillage Research*, *47*(1–2), 37–42. https://doi.org/10.1016/s0167-1987(98)00070-1

Schaap, M. G., & Leij, F. J. (2000). Improved prediction of unsaturated hydraulic conductivity with the Mualem-van Genuchten model. *Soil Science Society of America Journal*, *64*(3), 843–851. https://doi.org/10.2136/sssaj2000.643843x

Schaap, M. G., Leij, F. J., & van Genuchten, M. T. (2001). ROSETTA: A computer program for estimating soil hydraulic parameters with hierarchical pedotransfer functions. *Journal of Hydrology*, *251*(3–4), 163–176. https://doi.org/10.1016/s0022-1694(01)00466-8

Schneider, M., & Goss, K. U. (2012). Prediction of the water sorption isotherm in air dry soils. *Geoderma*, *170*, 64–69. https://doi.org/10.1016/j.geoderma.2011.10.008

Shen, C. P., Appling, A. P., Gentine, P., Bandai, T., Gupta, H., Tartakovsky, A., et al. (2023). Differentiable modelling to unify machine learning and physical models for geosciences. *Nature Reviews Earth & Environment*, *4*(8), 552–567. https://doi.org/10.1038/s43017-023-00450-9

Šimůnek, J., Šejna, M., Saito, H., Sakai, M., & Genuchten, M. T. V. (2008). The HYDRUS-1D software package for simulating the one-dimensional movement of water, heat. *Multiple Solutes in Variably-Saturated Media*.

Taccari, M. L., Wang, H., Goswami, S., De Florio, M., Nuttall, J., Chen, X. H., & Jimack, P. K. (2024). Developing a cost-effective emulator for groundwater flow modeling using deep neural operators. *Journal of Hydrology*, *630*, 130551. https://doi.org/10.1016/j.jhydrol.2023.130551

Tóth, B., Weynants, M., Nemes, A., Makó, A., Bilas, G., & Tóth, G. (2015). New generation of hydraulic pedotransfer functions for Europe. *European Journal of Soil Science*, *66*(1), 226–238. https://doi.org/10.1111/ejss.12192

Tsai, W. P., Feng, D. P., Pan, M., Beck, H., Lawson, K., Yang, Y., et al. (2021). From calibration to parameter learning: Harnessing the scaling effects of big data in geoscientific modeling. *Nature Communications*, *12*(1), 5988. https://doi.org/10.1038/s41467-021-26107-z

Tuller, M., & Or, D. (2005). Water films and scaling of soil characteristic curves at low water contents. *Water Resources Research*, *41*(9). https://doi.org/10.1029/2005wr004142

Tuller, M., Or, D., & Dudley, L. M. (1999). Adsorption and capillary condensation in porous media: Liquid retention and interfacial configurations in angular pores. *Water Resources Research*, *35*(7), 1949–1964. https://doi.org/10.1029/1999wr900098

Turek, M. E., Pullens, J. W. M., Meurer, K. H. E., Lima, E. M., Mehdi-Schulz, B., & Holzkämper, A. (2025). Pedotransfer functions versus model structure: What drives variance in agro-hydrological model results? *European Journal of Soil Science*, *76*(2), e70088. https://doi.org/10.1111/ejss.70088

Van Genuchten, M. T. (1980). A closed-form equation for predicting the hydraulic conductivity of unsaturated soils. *Soil Science Society of America Journal*, *44*(5), 892–898. https://doi.org/10.2136/sssaj1980.03615995004400050002x

Van Genuchten, M. T. (1987). A numerical model for water and solute movement in and below the root zone. In *Paper presented at the unpub research report, U S salinity laboratory*.

Van Looy, K., Bouma, J., Herbst, M., Koestel, J., Minasny, B., Mishra, U., et al. (2017). Pedotransfer functions in Earth System science: Challenges and perspectives. *Reviews of Geophysics*, *55*(4), 1199–1256. https://doi.org/10.1002/2017rg000581

Vereecken, H., Amelung, W., Bauke, S. L., Bogena, H., Brüggemann, N., Montzka, C., et al. (2022). Soil hydrology in the Earth system. *Nature Reviews Earth & Environment*, *3*(9), 573–587. https://doi.org/10.1038/s43017-022-00324-6

Vereecken, H., Diels, J., Van Orshoven, J., Feyen, J., & Bouma, J. (1992). FUNCTIONAL-EVALUATION of pedotransfer functions for the estimation of soil hydraulic-properties. *Soil Science Society of America Journal*, *56*(5), 1371–1378. https://doi.org/10.2136/sssaj1992.03615995005600050007x

Vereecken, H., Maes, J., Feyen, J., & Darius, P. (1989). Estimating the soil-moisture retention characteristic from texture, bulk-density, and carbon content. *Soil Science*, *148*(6), 389–403. https://doi.org/10.1097/00010694-198912000-00001

Vereecken, H., Weynants, M., Javaux, M., Pachepsky, Y., Schaap, M. G., & van Genuchten, M. T. (2010). Using pedotransfer functions to estimate the van genuchten-mualem soil hydraulic properties: A review. *Vadose Zone Journal*, *9*(4), 795–820. https://doi.org/10.2136/vzj2010.0045

Wang, Y., Ma, R., & Vereecken, H. (2025). A generalized framework to describe unimodal and bimodal soil hydraulic properties over full water saturation range. *Water Resources Research*, *61*(2), e2024WR038450. https://doi.org/10.1029/2024wr038450

Wang, Y. Q., Jin, M. G., & Deng, Z. J. (2018). Alternative model for predicting soil hydraulic conductivity over the complete moisture range. *Water Resources Research*, *54*(9), 6860–6876. https://doi.org/10.1029/2018wr023037

Wang, Y. Q., Ma, J. Z., & Guan, H. D. (2016). A mathematically continuous model for describing the hydraulic properties of unsaturated porous media over the entire range of matric suctions. *Journal of Hydrology*, *541*, 873–888. https://doi.org/10.1016/j.jhydrol.2016.07.046

Wang, Y. Q., Ma, J. Z., Zhang, Y. L., Zhao, M. Z., & Edmunds, W. M. (2013). A new theoretical model accounting for film flow in unsaturated porous media. *Water Resources Research*, *49*(8), 5021–5028. https://doi.org/10.1002/wrcr.20390

Wang, Y. Q., Ma, R., & Zhu, G. F. (2023). Representation of the influence of soil structure on hydraulic conductivity prediction. *Journal of Hydrology*, *619*, 129330. https://doi.org/10.1016/j.jhydrol.2023.129330

Wang, Y. Q., Zhou, J. L., Ma, R., Zhu, G. F., & Zhang, Y. Y. (2022). Development of a new pedotransfer function addressing limitations in soil hydraulic models and observations. *Water Resources Research*, *58*(6), e2021WR031406. https://doi.org/10.1029/2021wr031406

Weber, T. K. D., Finkel, M., Gonçalves, M. D., Vereecken, H., & Diamantopoulos, E. (2020). Pedotransfer function for the brunswick soil Hydraulic property model and comparison to the van genuchten-mualem model. *Water Resources Research*, *56*(9), e2019WR026820. https://doi.org/10.1029/2019wr026820

Weber, T. K. D., Weihermüller, L., Nemes, A., Bechtold, M., Degré, A., Diamantopoulos, E., et al. (2024). Hydro-pedotransfer functions: A roadmap for future development. *Hydrology and Earth System Sciences*, *28*(14), 3391–3433. https://doi.org/10.5194/hess-28-3391-2024

Weihermuller, L., Lehmann, P., Herbst, M., Rahmati, M., Verhoef, A., Or, D., et al. (2021). Choice of pedotransfer functions matters when simulating soil water balance fluxes. *Journal of Advances in Modeling Earth Systems*, *13*(3), e2020MS002404. https://doi.org/10.1029/2020ms002404

Werbos, P. J. (1990). Backpropagation through time - what it does and HOW to do it. *Proceedings of the IEEE*, *78*(10), 1550–1560. https://doi.org/10.1109/5.58337

Zhang, Y. G., & Schaap, M. G. (2017). Weighted recalibration of the Rosetta pedotransfer model with improved estimates of hydraulic parameter distributions and summary statistics (Rosetta3). *Journal of Hydrology*, *547*, 39–53. https://doi.org/10.1016/j.jhydrol.2017.01.004

Zhang, Y. G., Schaap, M. G., & Zha, Y. Y. (2018). A high-resolution global map of soil hydraulic properties produced by a hierarchical parameterization of a physically based water retention model. *Water Resources Research*, *54*(12), 9774–9790. https://doi.org/10.1029/2018wr023539

Zheng, Y., Zhang, L., Xiao, J., Yuan, W., Yan, M., Li, T., et al. (2018). Sources of uncertainty in gross primary productivity simulated by light use efficiency models: Model structure, parameters, input data, and spatial resolution. *Agricultural and Forest Meteorology*, *263*, 242–257. https://doi.org/10.1016/j.agrformet.2018.08.003

Zhou, J., Wang, Y., Qi, P., Ma, R., Vereecken, H., Minasny, B., & Zhang, Y. (2025). Soil Physics-Informed Neural Networks to estimate bimodal soil hydraulic properties. *Water Resources Research*, *61*(10), e2024WR039337. https://doi.org/10.1029/2024wr039337

Zhu, G., Li, X., Ma, J., Wang, Y., Liu, S., Huang, C., et al. (2018). A new moving strategy for the sequential Monte Carlo approach in optimizing the hydrological model parameters. *Advances in Water Resources*, *114*, 164–179. https://doi.org/10.1016/j.advwatres.2018.02.007